TURBOMACHINERY & PUMP SYMPOSIA | HOUSTON, TX
DECEMBER 14-16, 2021
SHORT COURSES: DECEMBER 13, 2021

TUTORIAL – SCO_2 COMPRESSION

Stefan D. Cich
Group Leader
Southwest Research Institute
San Antonio, Texas, USA

J. Jeffrey Moore
Institute Engineer
Southwest Research Institute
San Antonio, Texas, USA

Chris Kulhanek
Research Engineer
Southwest Research Institute
San Antonio, Texas, USA

Jason P. Mortzheim
Senior Engineer, Mechanical
GE Global Research
Niskayuna, New York, USA

Stefan Cich is a Group Leader in the Machinery Section at Southwest Research Institute (SwRI) in San Antonio, TX. He holds a B.S. in Aerospace Engineering from the University of Texas at Austin. His professional experience over the last 9 years has been focused around the design, analysis, and development of high pressure equipment and turbomachinery. His first job for two years focused on high pressure hydraulic fracturing equipment. While at SwRI, his main focus has been on various advanced turbines and compressors for a variety of applications. Much of it has been on the development and testing of equipment for use in super critical CO_2 power cycles. This includes multiple 16 MWe turbines, 2.5 MW compressors, 5.5 MW to 55 MW recuperators, and a 2 MW heater along with all the necessary equipment to fully operate a power loop. Through all of this, he has gained experience in various ASME and API codes, design and manufacturing of advanced equipment through advanced manufacturing processes, complex stress and thermal analysis of high temperature and high pressure equipment, and testing and operating procedures of new age power cycles.

Dr. Jeffrey Moore is an Institute Engineer in the Machinery Section at Southwest Research Institute in San Antonio, TX. He holds a B.S., M.S., and Ph.D. in Mechanical Engineering from Texas A&M University. His professional experience over the last 30 years includes engineering and management responsibilities related to centrifugal compressors and gas turbines at Solar Turbines Inc. in San Diego, CA, Dresser-Rand (now Siemens Energy) in Olean, NY, and Southwest Research Institute in San Antonio, TX. His interests include advanced power cycles and compression methods, rotordynamics, seals and bearings, computational fluid dynamics, finite element analysis, machine design, controls, aerodynamics, and oxy-combustion. He has authored over 40 technical papers related to turbomachinery and has four patents issued. Dr. Moore has held positions as the Vanguard Chair of the Structures and Dynamics Committee and Chair of Oil and Gas Committee for IGTI Turbo Expo. He has also served as the Associate Editor for the Journal of Tribology and a member of the IGTI SCO2 Committee, Turbomachinery Symposium Advisory Committee, the IFToMM International Rotordynamics Conference Committee, and the API 616 and 684 Task Forces.

Mr. Jason Mortzheim is a senior mechanical engineer at the GE Global Research Center in Niskayuna, NY. He has a B.S. in aeronautical engineering from Rensselaer Polytechnic Institute and a M.S. in aerospace engineering from Georgia Institute of Technology. His area of research has been centered on improving fossil power combined cycle plant efficiency including both steam and gas turbines. Mr. Mortzheim initial area of research focused around advanced seal designs where he has held various roles spanning his 19 year professional career. He has utilized computational methods, both commercial CFD and in-house flow solvers, advanced experimental campaigns including industry leading test rig designs, complete to post commercial operation validation to develop state of the art seal technology ranging from brush seals to film riding seals. Mr. Mortzheim is currently the Principal Investigator for DoE contract, EE0007109 related to advanced sCO2 power cycle compression technology and the GE Principal Investigator supporting DoE contract, FE0028979, 10 MWe sCO2 Pilot Plant Test Facility.

ABSTRACT

Supercritical Carbon Dioxide (sCO_2) power cycles are a transformational technology for the energy industry, providing higher thermal efficiency compared to traditional heat-source energy conversion including conventional fossil and alternative energy sources. The novel cycle significantly reduces capital costs due to smaller equipment footprints and design modularity. In addition, it allows for rapid cyclic load and source following to balance solar and wind energy power swings. Compressing CO_2 is not novel, but mostly at lower vapor pressures, and at higher pressure and lower temperatures as a liquid. Compression near the dome (near critical pressure and temperature) is a new interest that has many advantages and challenges. The key advantage is the low head requirement when compressing near the CO_2 dome (95°F [35°C] and 1,233 psi [8.5 MPa]). To pressurize from 1,233 psi (target inlet pressure of power cycles) to 3,916 psi (27.0 MPa), only a single high-speed compressor stage is required. This low head requirement means less power is required to compress and leads to an increase in thermal efficiency of these cycles. High-efficiency compression technology can reduce the power of Enhanced Oil Recovery (EOR) and Carbon Capture and Sequestration (CCS) applications.

This type of compression also brings many challenges. A compressor for this application pushes many current technology limits, including but not limited to: pressure rise per stage, bearing technologies, sealing technologies, damping, rotordynamics, compact machinery packaging, and high-density, high-speed compression. In addition, when compressing near the CO_2 dome, there are large swings in density for slight changes in temperature. This is a unique challenge not observed when CO_2 is pumped as a liquid or compressed as a vapor. Due to these large changes in density, range extension is required to maintain high compression efficiency and controlled mass flow over a range of operating temperatures.

Recent testing finished on a state-of-the-art sCO_2 compressor operating near the dome that was designed, manufactured, and tested by Southwest Research Institute (SwRI) and General Electric Global Research (GE-GRC). This tutorial will highlight many of the unique aspects of the design, especially those challenges and decisions that were focused on high pressure ratio compression stages, high-density and high-speed flow, special rotordynamic considerations, and the overall challenges of compact high-pressure turbomachinery. It will then cover how the design and analysis translated to testing with a real gas that experiences rapid changes in fluid properties for minimal fluctuations in temperature. In addition, due to its need for compact, high-power, and high-speed machinery, the development of sCO_2 machinery aids in the development of many advanced components and hardware that can also be used in other applications. This includes high-pressure and high-temperature end seals, zero- to low-emission seals, hermetically sealed systems with gas or magnetic bearings, high-pressure single stage compressors, range extension technologies like variable Inlet Guide Vanes (IGVs), and high-density and high-critical speed ratio operation.

Why sCO_2?

sCO_2 is of great interest and research is underway through commercial development and government funding. It is being pursued through the development of advanced power cycles to lead to low-emission, high-efficiency power production. Current interests are centered on Concentrated Solar Power (CSP) with the Recompression Brayton Cycle (RCBC), Waste Heat Recovery (WHR) with the simple recuperated cycle, and Oxy-Combustion with the Allam Cycle. In addition to power production, there is also interest in sCO_2 technologies for use with Enhanced Oil Recovery (EOR) and Carbon Capture and Sequestration (CCS) applications to improve the efficiency of pipeline distribution and downhole injection.

However, the range at which these compressors operate is a big challenge mechanically due to the rapid change in fluid properties near the critical point. The critical point of a fluid defines the pressure and temperature at which the fluid enters the supercritical phase (87.8°F [31°C] and 1,072 psia [7.39 MPa] [Figure 1] for CO_2). Supercritical phases have fluid behavior that is representative of a gas and liquid and exhibit strong real gas (non-ideal) behavior. The other more common fluid that also sees similar behavior is water, which is used in Steam Rankine Cycles. The difference with Supercritical Steam (sH_2O) and sCO_2, is that the critical point for water is at a much higher temperature >698°F [370°C]. The 87.8°F critical point for CO_2 is important because it is near standard ambient conditions. This is important in power cycles because this is achieved with dry or wet cooling without the need for expensive chilling systems. For pipeline applications, these temperatures will be reached while the CO_2 is distributed in a pipeline without any heating or cooling. In terms of heat rejection, chilling is detrimental to a power cycle due to the low Coefficient of Performance (COP) [Heat Rejected divided by Input Power] compared to atmospheric cooling. For pipeline applications, chilling or heating causes a direct increase in operating expenses.

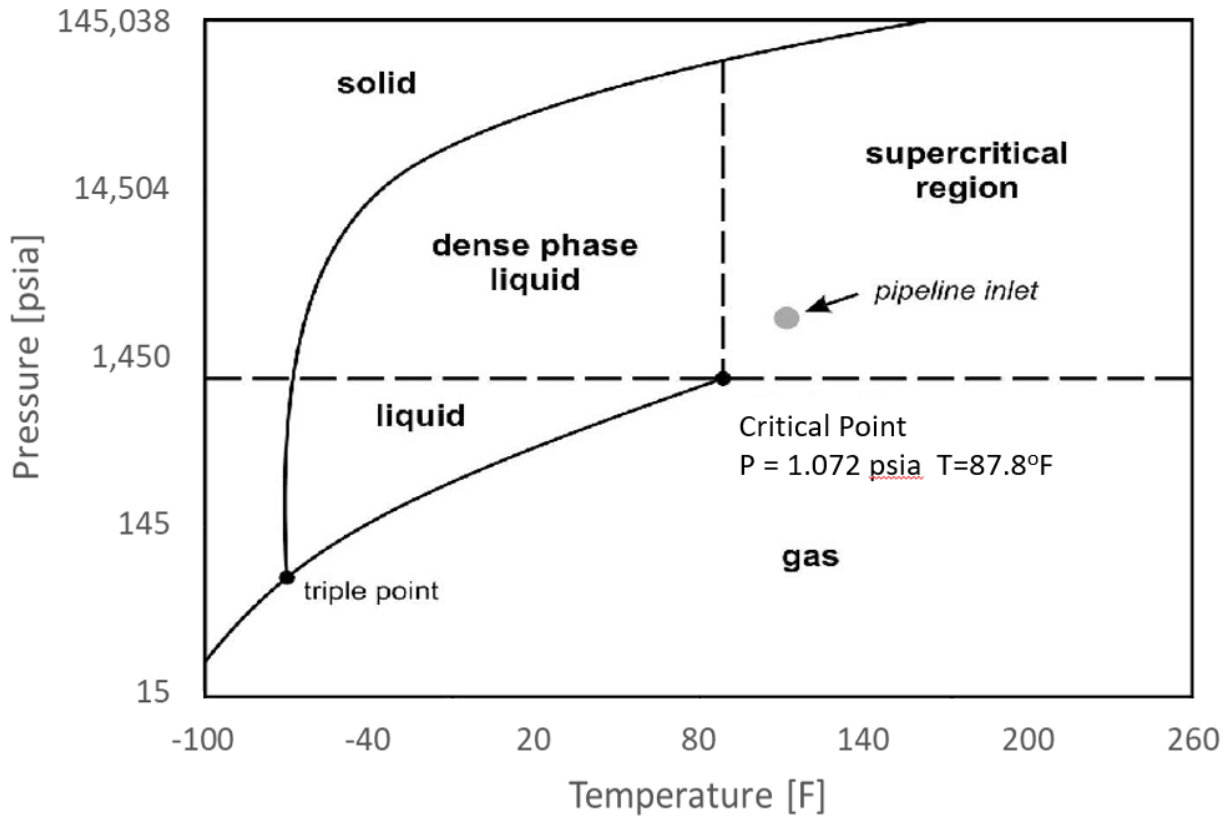

Figure 1 - CO_2 Phase Diagram (Pressure vs Temperature) [1]

To understand why this area of operation is a challenge, it is necessary to look at the change in fluid properties with temperature of CO_2. Figure 2 shows density comparisons and Figure 3 displays enthalpy variations. Three pressures are discussed for comparison: 300 psia (2.1 MPa), 1,075 psia (7.4 MPA), and 1,200 psia (8.3 MPa). A pressure of 300 psia will be representative of typical gas pressures in CO_2 compression applications, 1075 psia is very close to the critical pressure of CO_2, and 1,200 psia is typically used for dome avoidance in power and compression applications to avoid rapid property changes of CO_2.

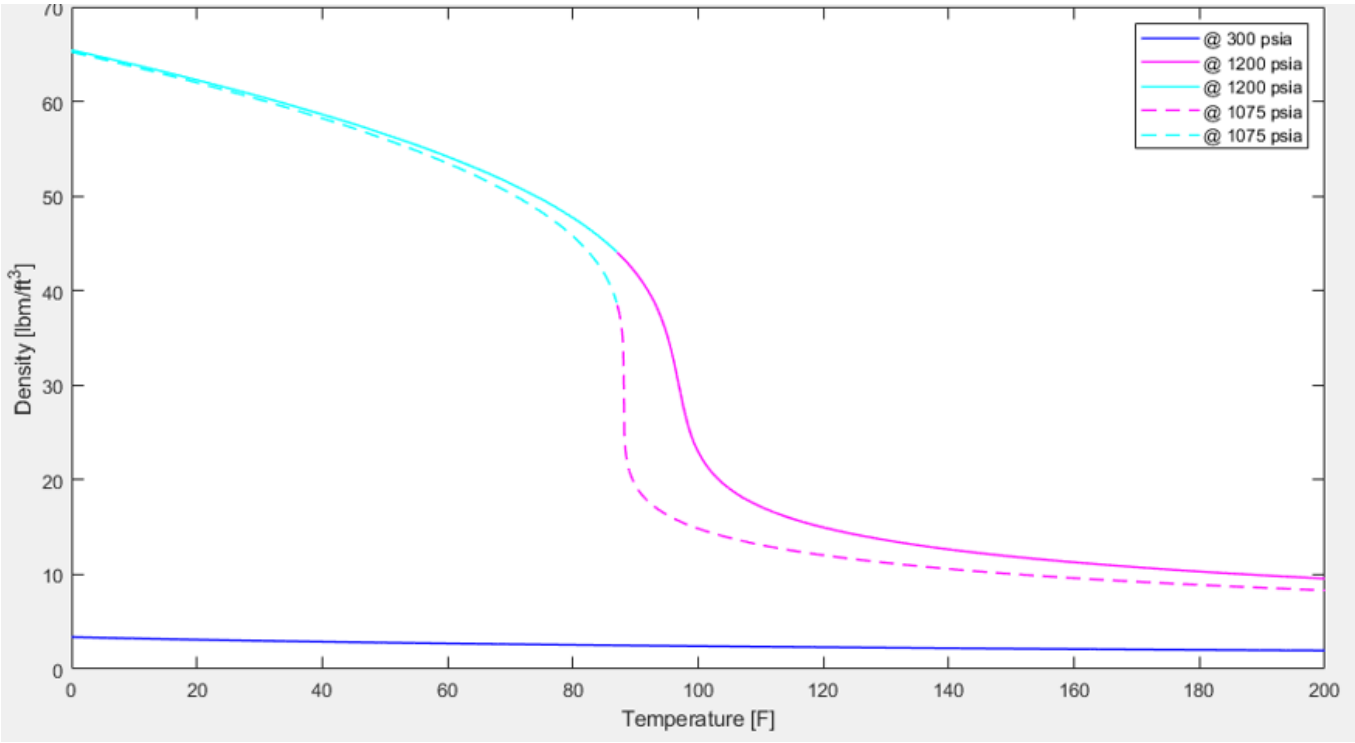

Figure 2 – CO_2 Density vs Temperature to Highlight Impact on Flow Density near the CO_2 Critical Point. With Systems based on Volume Flow, there will be a large impact on Mass Flow

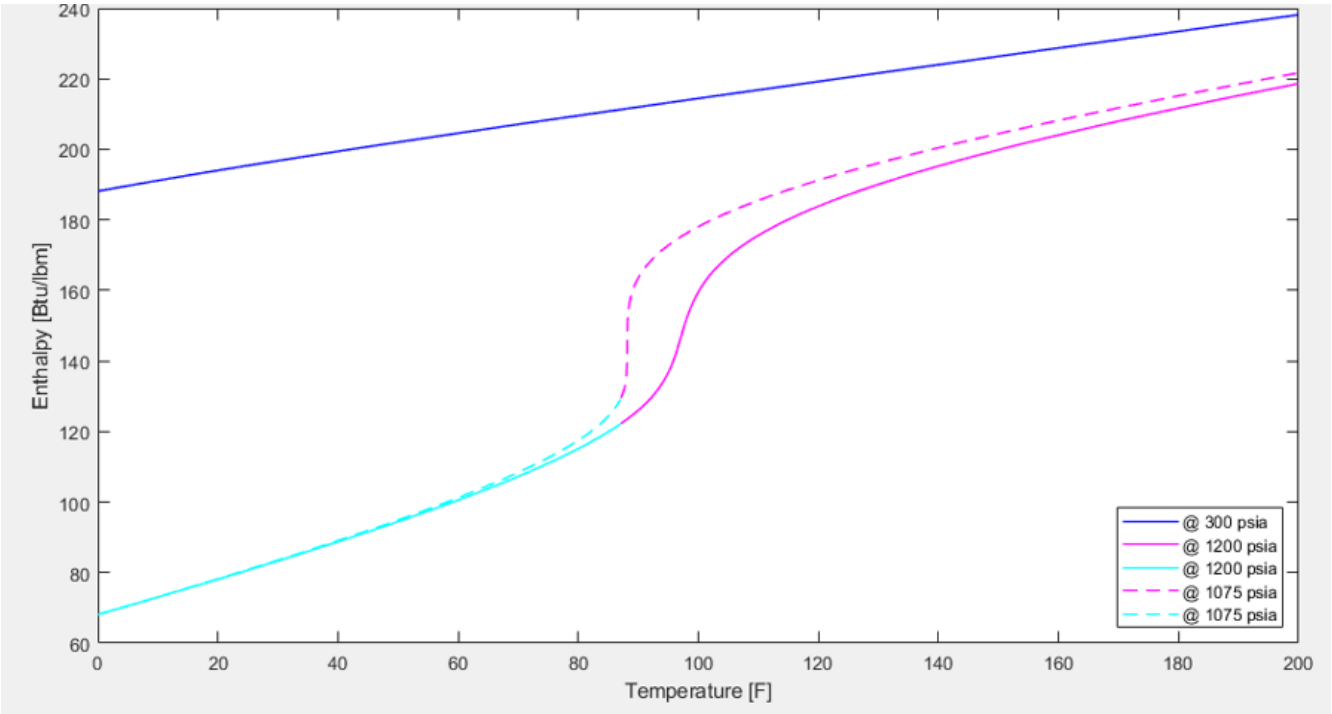

Figure 3 – CO_2 Enthalpy vs Temperature to Highlight Property Variations near the CO_2 Critical Point

The most important sections are the temperatures between 80-100ºF (27 to 38ºC) which sees the rapid transition between dense-phase to supercritical CO_2. In past CO_2 application, this area of operation was typically avoided because of the uncertainty in fluid properties and potential for two-phase flow. To avoid this region, reduced pressures (below the critical pressure) or temperatures (below the critical temperature) are desired. This leads to gas compression (high head per unit mass) or liquid pumping (increased capital and operating expenses [CAPEX and OPEX] for chilling capacity). Because of this, there is a strong need for the development of technology that can operate near the dome to both increase compression efficiency and reduce capital cost by removing the need for expensive chilling or heating systems. Figure 4 highlights the required Isentropic Head to achieve a pressure ratio of 3X at different operating pressures. As expected, more head (compression power) is required for gas whereas liquid requires the least amount of head. Due to density remaining

near constant at liquid conditions, there is very little change in head with pressure. Near the critical point (88ºF [31.1ºC]), there is a sudden change in required isentropic head. For peak compression efficiency and lowest required power, it is desirable to stay to the left of this point based on minimum temperature that can be achieved through the use of atmospheric cooling (dry or water).

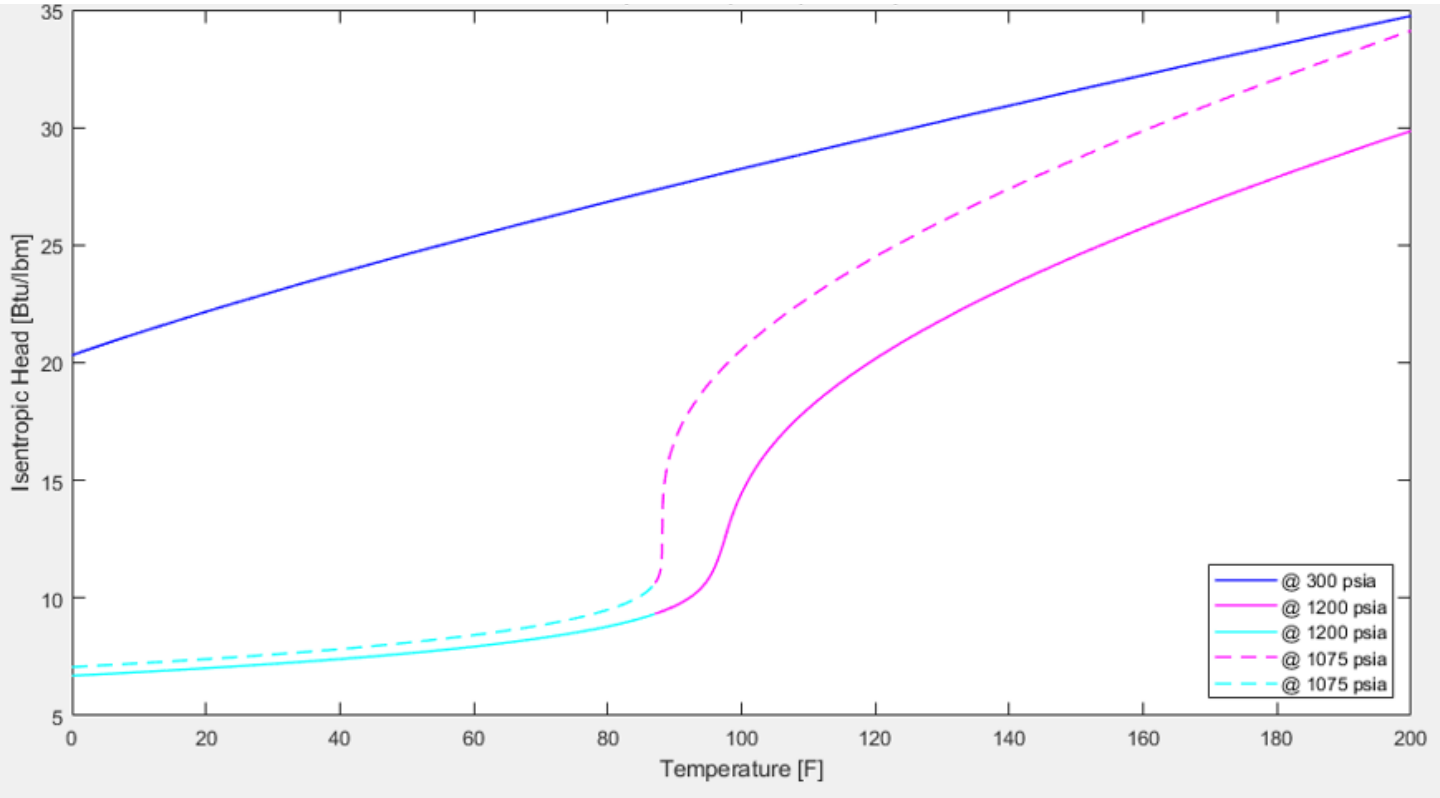

Figure 4 - Isentropic Head vs Temperature for a 3X Pressure Ratio

In terms of compressor design, this leads to two main options (when considering centrifugal units): a low-speed, multi-stage unit (dense phase pump) or a high-speed, single-stage unit. A low-speed unit provides the advantage of being relatively low-risk in terms of mechanical performance, primarily rotordynamic concerns with a dense fluid. However, low-speed units will typically see lower overall efficiency in addition to larger losses from windage, seal leakage, and secondary losses. In addition, many compression stages leads to a larger and more expensive machine. A high-speed, single-stage unit will typically have a wider range of higher efficiency and less secondary losses, but will be operating in a high-risk area due to rotordynamic concerns.

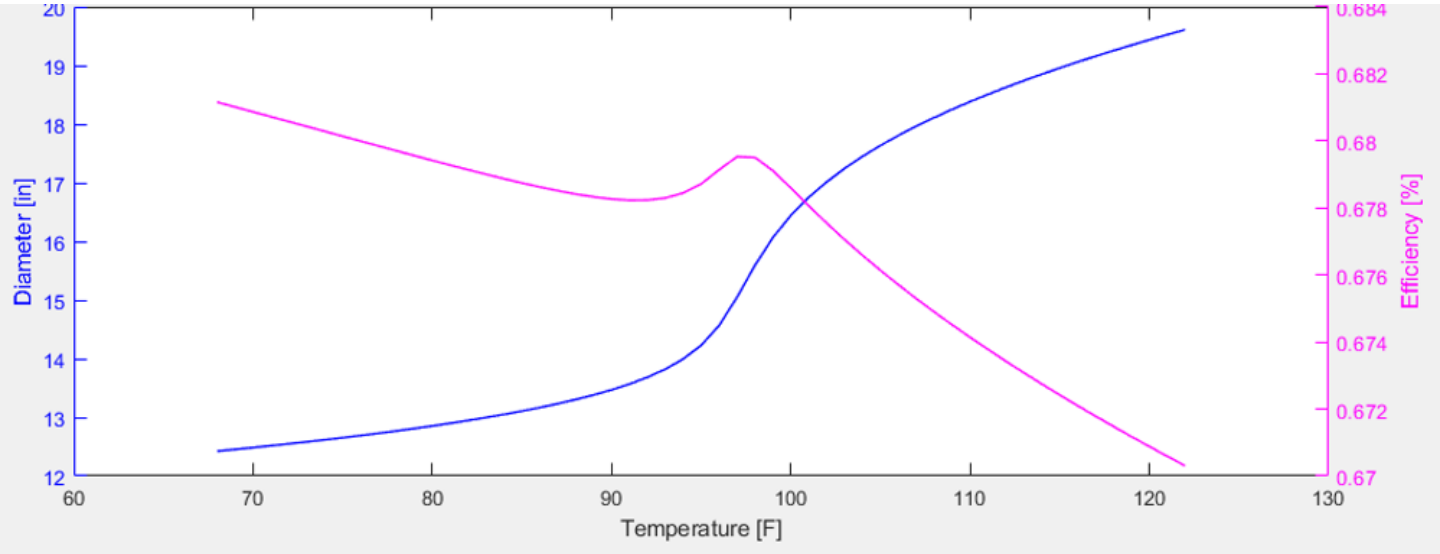

Figure 5 - Balje Comparison (Impeller Diameter and Compressor Efficiency) vs Suction Temperature at 1,200 psia (8.3 MPa) and 100 lbm/s (45 kg/s) inlet for a low-speed, multi-stage Compressor

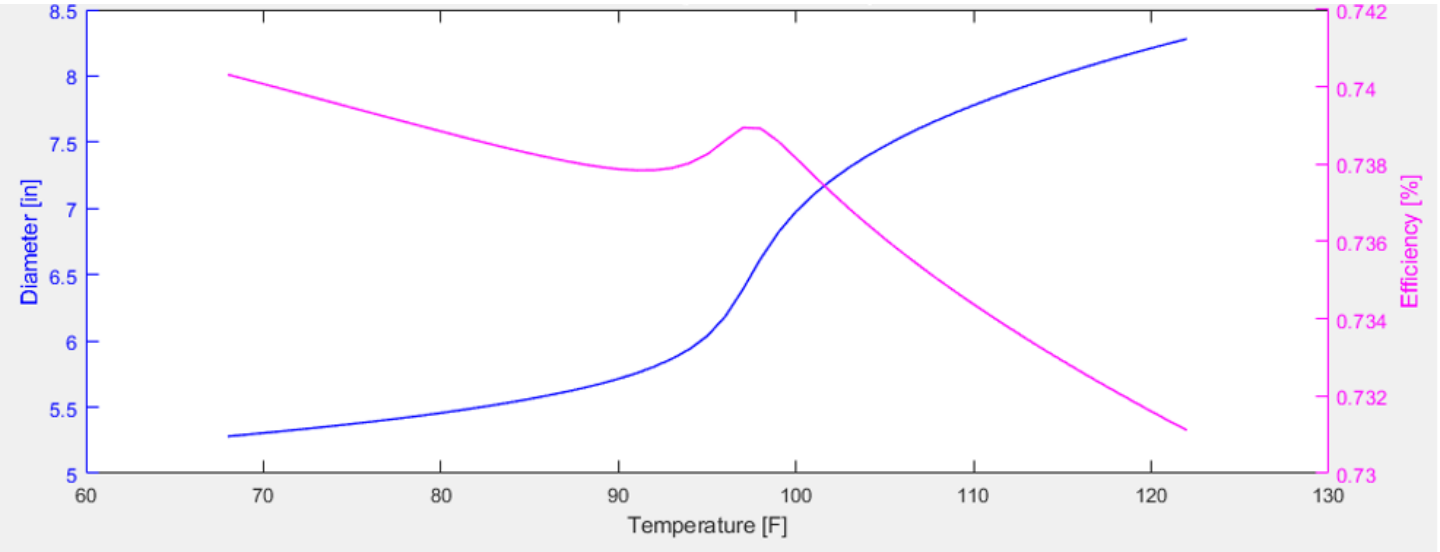

Figure 6 - Balje Comparison (Impeller Diameter and Compressor Efficiency) vs Suction Temperature at 1,200 psia (8.3 MPa) and 100 lbm/s (45 kg/s) for a high-speed, single-stage Compressor

While the focus of this tutorial will be on centrifugal units for sCO_2 compression, it is important to note that Reciprocating Compressors (Recips) are used in this area of operation (above critical pressure and downhole). Compared to Recips, centrifugal compressors can deliver higher flow in a smaller overall package with less wear and tear on components, primarily seals. This leads to longer Mean Time Between Failures (MTBF), higher reliability, and an overall smaller compression package that will reduce costs and required space. When considering EOR or CCS, cost and space are a premium, and finding a reliable and cost effective solution is necessary to continue to deploy the technology. Compared to liquid pumps a single stage centrifugal wheel has the advantage of reduced stage count and overall machine complexity. Fewer stages and higher speeds leads to reduced size and cost, and increased efficiency. This all benefits CAPEX and OPEX for a reduced cost compression package. In addition, a single stage will require flow range extensions (variable IGVs here) on only one stage of compression, reducing overall package complexity cost while increasing the range of operation.

As previously mentioned, a dense-phase unit will typically be a low-speed multi-stage unit that will require chilling prior to compression / pumping. This is to prevent multi-phase flow and cavitation inside the unit. Unlike water cooling, which has a COP in excess of 25, chilling typically has a COP between 3.5 and 5.5. While liquid compression does require less compression power, it is important to understand the heat rejection required to achieve those conditions and include in total power. Highlighted in Figure 7, chilling requirements become detrimental to overall operating costs at higher ambient temperature (between orange and gray lines). Total power calculations:

- Blue Line [Compression Power (No Chilling)]
  - Enthalpy Change at 85% Isentropic Efficiency from 1,300 to 2,175 psia (9.0 to 15.0 MPa) at each pipeline temperature
- Orange and Grey Line [Compression Power + Chilling]
  - Chilling Power = Enthalpy Change from Pipeline Temperature down to 32°F divided by specified COP
  - Compression Power = Enthalpy Change at 85% Isentropic Efficiency from 1,300 to 2,175 psia at each pipeline temperature

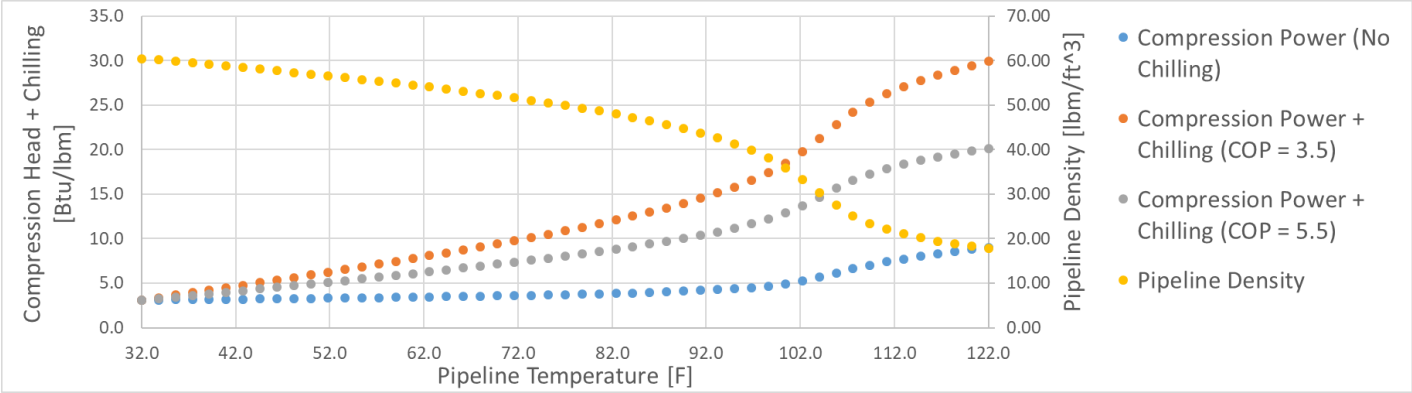

Figure 7 - Compression + Chilling Requirements for Varying Pipeline Temperatures from 1,300 (9.0 MPa) to 2,175 psia (15 MPa), Chilling to 32°F (0°C) and No Chilling

Figure 8 highlights two different CCS compression cycles (near isothermal with cooling after every impeller and back-to-back barrel design with cooling after each stage) and where a sCO_2 compressor can fit into a standard compression cycle, primarily at the last stage where a single stage, sCO_2 compressor can replace a larger multi-stage dense-phase pump. Total power can be reduced significantly by avoiding the need to cool below the critical point. These compression options are described further in Moore, et al., 2011 [1].

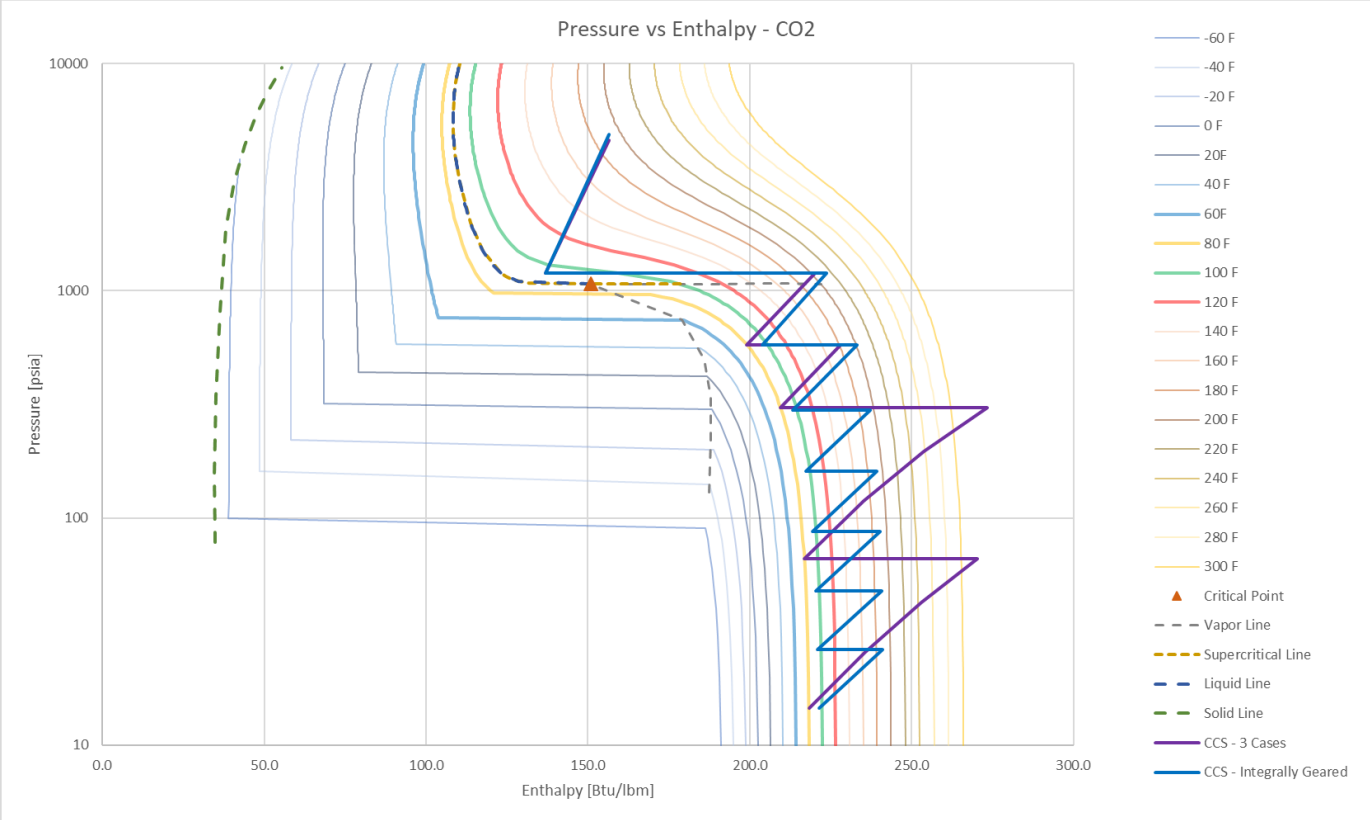

Figure 8 - Semi-Isothermal Compression vs Conventional Compression

What are the Challenges with sCO_2 Compression?

Before going into the mechanical design of sCO_2 machinery, it is important to understand the main challenges associated with these applications. Most of the challenges are associated with the high fluid density at colder conditions with CO_2 approaching that of water, but also in the density fluctuations from 68ºF to 122ºF (20 to 50ºC) experienced in various locations and seasons around the world. To meet required performance (pressure and supplied mass flow), flow range extensions are required. In terms of fluid density, Figure 9 highlights one of the challenges with compressing CO_2. For small temperature variations, around 86º to 104ºF (30 to 40ºC), there are large changes in density (around 10-15% / ºF). For a fixed mass flow system, the small changes in temperature (large density swings) will push a compressor toward surge with the large reduction in volume flow. In addition, there are variations in speed of sound (Figure 10) which will lead to choked flow of characteristic speed lines shifting left (reducing). In terms of density, the Apollo point on the Fulton Chart (Figure 9) shows that the combination of Gas Mean Density, the average density of suction and discharge flow, and Critical Speed Ratio (CSR), the ratio of Max Continuous Speed over the 1st critical speed, is far outside the experience range. This leads to the multi-stage low-speed design discussed earlier as the simpler approach. To look at reduced span, reduced cost, and higher efficiencies, there is a need to enter regions outside of common experience.

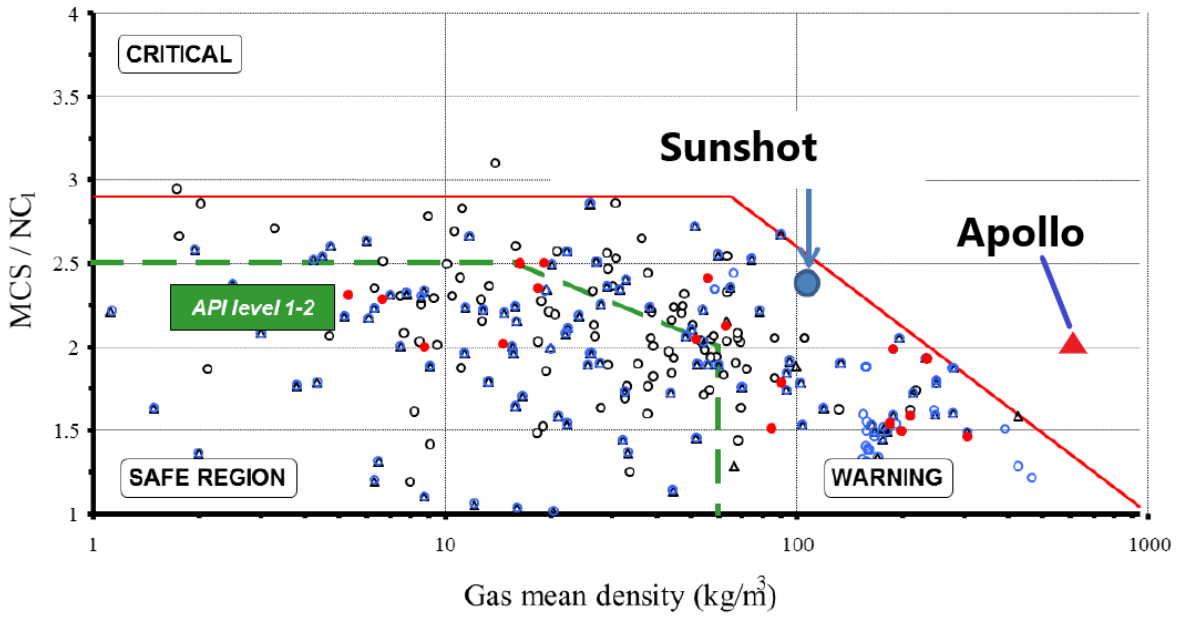

Figure 9 - Rotordynamic Experience Chart from [2] with Sunshot Turbine and Apollo Compressor Rotor Added [2]

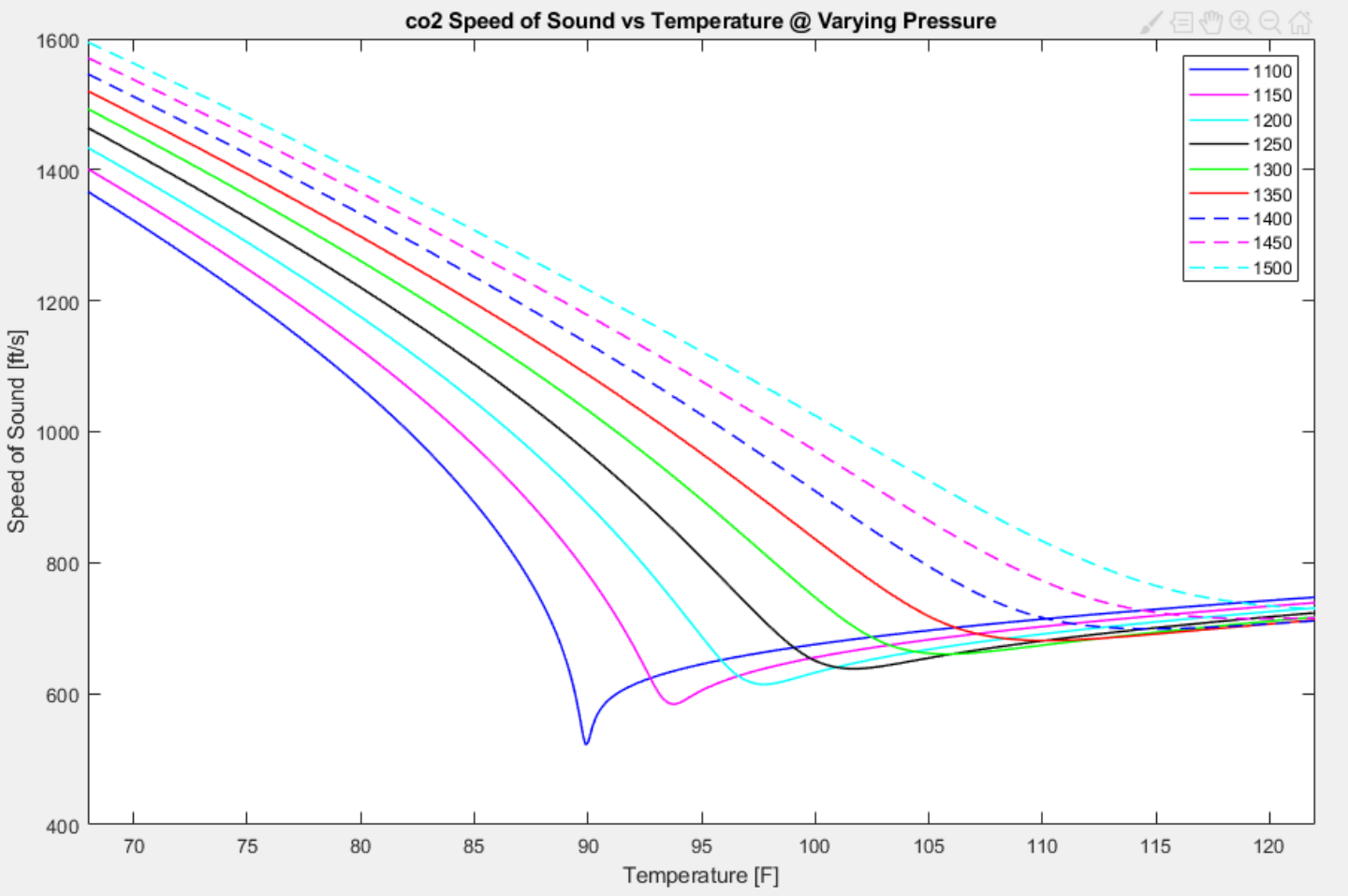

Figure 10 - Speed of Sound Variation with Temperature and Pressure to Understand potential issues with Choking when Compressing near the CO_2 Dome

Because of these aspects of sCO_2 compression, there is a need to develop a high-efficiency, high-speed compressor that can handle the large density swings (flow-range extension), high fluid densities, and operating above the 1st bending critical (high-damping). In addition

to the density challenges, there is also the challenge of designing a high differential pressure, single stage compressor. This high pressure rise creates challenges for sealing, deformation, diaphragm stresses, etc. Special consideration has to be taken in the case layout and rotor design to account for sufficient axial and radial space to accommodate this large pressure differential.

To address these concerns, the tutorial will take a look at the mechanical design of a current sCO_2 compressor that has been successfully manufactured and tested along with lessons learned that led to successful completion of the program.

EXAMPLE COMPRESSOR

The program which this sCO_2 compressor was developed under was focused on the development of a Recompression Brayton Cycle (RCBC) for use with Concentrated Solar Power (CSP) technologies. Some of the components and operating conditions are unique to this power cycle, but many of the advantages and challenges for the use of a sCO_2 compressor in this power cycle are also applicable to the use of this technology for other applications, including CCS and EOR. The RCBC is an attractive cycle for sCO_2 that could meet the relative efficiencies of steam based Rankine cycles. To meet these efficiencies, the cycle requires low and high temperature recuperators, turbine inlet temperatures between 1,112-1,400ºF (600-760ºC), a main compressor, and a bypass compressor. There is an ideal balance between the flow split on the main compressor and bypass compressor. While the lower temperature flow requires less power to compress, the higher temperature will increase the effectiveness of recuperation in the loop [3]-[6]. Other US DOE projects have focused on the cost and effectiveness of the recuperators and the design and development of the high temperature sCO_2 turbine [7]-[9]. The US DOE Apollo program's focus is on the design and testing of the main compressor for this RCBC.

The main compressor has a nominal operating point of 95ºF (35ºC) and 1,260 psi (86.9 bar). This design point is chosen as one of the optimal points for the RCBC due to its effect on the overall cycle efficiency for a desert environment. It is also above the critical point of CO_2 to avoid compressing liquid in the main compressor. Previous papers have reviewed and gone into the detail on compressor design limits with CO_2 and the advantage of compressing in the supercritical state rather than trying to pump in the liquid state [10]-[14]. For CCS and EOR, the goal will be to stay to the right of the CO_2 dome as shown in Figure 8. Staying to the right of the dome will avoid the potential for two-phase compression of CO_2 liquid and vapor and also require less cooling to achieve higher downhole pressures.

Density has a significant impact on rotordynamic behavior due to its effect on fluid forces. Shown in Figure 9, the Fulton Chart compares API requirements and experience in terms of CSR vs average gas density. For these relative densities, the usual choice would be a low-speed, dense-phase liquid pump, however, when looking at required cooling, this leads to a negative effect on overall efficiency, and will also lead to a much larger machine with more stages and increased secondary losses. By being able to compress in the supercritical phase, a high-speed, high-efficiency single stage wheel can be utilized to reduce the overall power required.

One of the unique challenges of this design and application, and the reason why the rotor is operating at a high CSR is because it was designed to package both the main compressor and bypass compressor in a single case. For this power cycle, by having both compressors packaged in a single case and also speed matched to the turbine, a directly coupled train could be designed that would reduce the overall footprint of the 10 MWe power block. This paper will take a detailed look at the mechanical design and testing of the compressor and will not focus on the aerodynamic performance.

ROTORDYNAMIC DESIGN

For this application, similar to the design of a sCO_2 Turbine [7], Integral Squeeze Film Damper (ISFD) bearings to improve rotordynamic performance are utilized [15]. At that time, the rotor design was based on a conventional approach as shown in Figure 11 and Figure 12, but due to design margin with the 3rd mode, the rotor layout was changed to create more separation margin between operating speed and the calculated modes. Configuration 1 has a separation margin of only 1.3% to the 3rd mode (1st bending) critical speed. This configuration had a more standard design in which the thrust collar was outboard of the journal bearing on the non-drive end (NDE) of the rotor, the coupling was outboard of the journal bearing on the drive-end (DE) of the rotor, dry gas seals (DGS) were directly inboard of the journal bearings, and the balance piston was between the bypass compressor suction and the DE DGS. Even though this compressor was a back-to-back design, a balance piston was needed to account for different sized impellers between the main and bypass compressor and for the use of only the main compressor. In addition, since these compressors were discharging to different points in the loop along with different suction conditions, there would be slight differences in pressure rise across each compressor during standard operation that could lead to thrust imbalance.

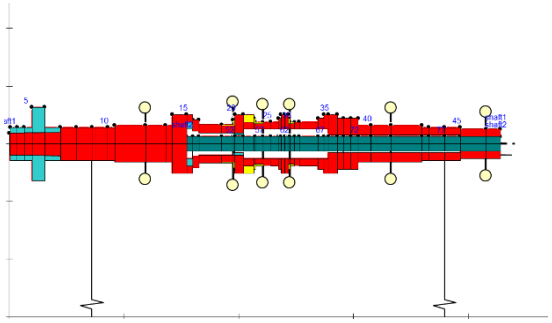

Figure 11 - Rotor Layout - Configuration 1 [16]

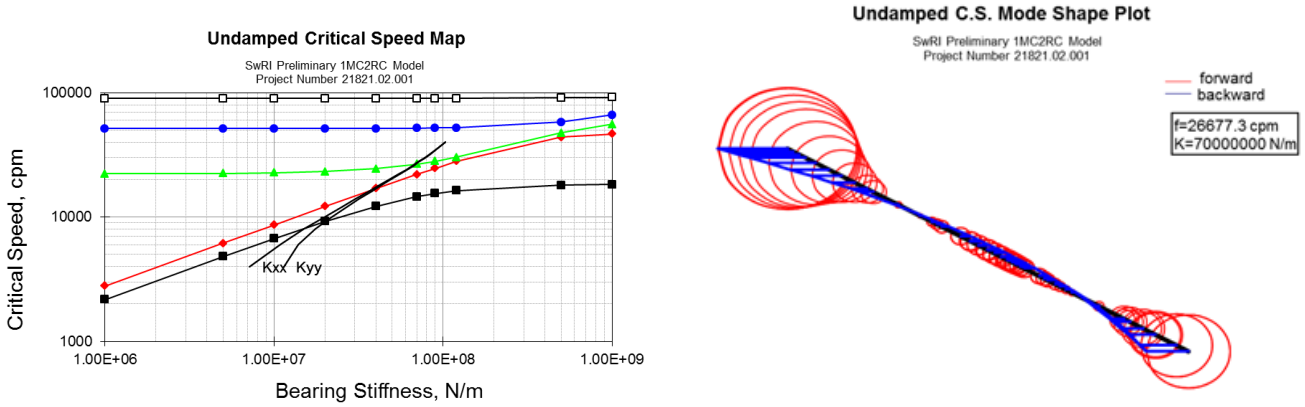

Figure 12 - Undamped Criticial Speed Map (Left) and 3rd Mode (Right) with 1.3% separation margin for Configuration 1 [16]

To improve this separation margin, the balance piston was moved in between the main compressor and bypass compressor to allow for significant damping in the middle of the rotor (Figure 13). Due to the high-pressure drop, mass flow, and density across the balance piston that is unique for sCO_2 compression, a balance piston seal can be beneficial to the overall stability of the machine. This is why a hole-pattern damper seal is used rather than a labyrinth seal. One disadvantage is that a hole-pattern seal requires larger clearances, when compared to a tooth on rotor and abradable stator, especially in the middle of the rotor where motion would have the highest amplitude. With increased damping, the mode only dropped by 500 cpm, increasing separation margin to 3.1%, with operation still above the 3rd mode.

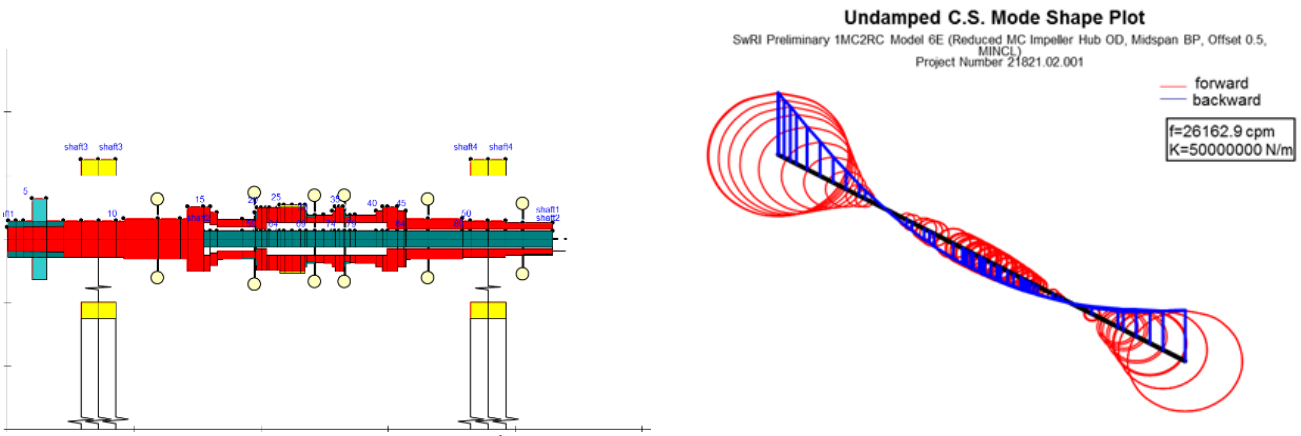

Figure 13 - Rotor Layout (Left) and 3rd Mode (Right) with 3.1 % Separation Margin for Configuration 2 [16]

For Configuration 3, Figure 14, the thrust bearing was moved inboard of the journal bearing due to a nodal point of the mode acting right at the journal bearing location. By moving the thrust bearing inboard and increasing the bearing span, the margin to the 3rd mode was increased. In addition to increasing the span, moving the thrust bearing inboard also reduced the overhung moment on the Non-Drive End (NDE) of the compressor, therefore increasing the 3rd mode. The main disadvantage of this approach is that journal bearing sizes are limited. For a small rotor like this, the static loads on the bearings are small, but larger bearings could provide more stiffness that would assist in limiting motion of the rotor with the potential for high vibrations due to the high-density flow and high-speed operation.

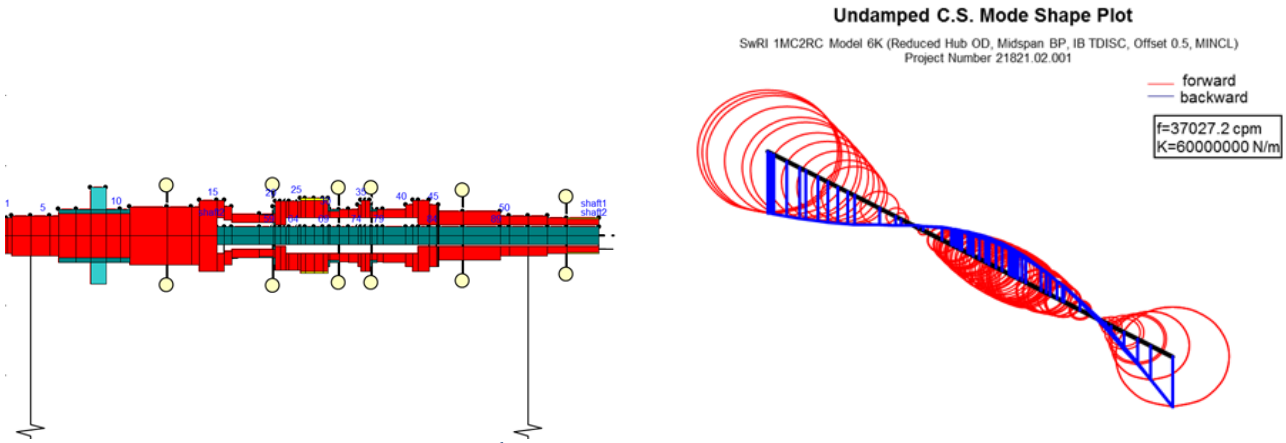

Figure 14 - Rotor Layout (Left) and 3rd Mode (Right) with 37% Separation Margin for Configuration 3 [16]

By moving the thrust bearing inboard, the 3rd undamped mode was increased significantly (37% margin). This allows for significant separation margin to operating speed and led to the final rotor configuration for this design. One of the challenges with moving the thrust bearing inboard is that some significant design changes were required for the original thrust bearing and thrust collar. By keeping the bearings the same size, the minimum diameter of the thrust collar was increased to be larger than the bearing diameter, rather than the largest diameter of the thrust collar taper being at the bearing diameter. This also prevents the potential of increasing radial bearing sizes if more stiffness is needed. Due to the current design envelope, the same size thrust bearing would have to be used to keep the same outer diameter and also the same required oil flow. In order to account for a larger diameter thrust collar, the thrust bearing inner diameter was increased, therefore decreasing the thrust capacity of the thrust bearing. This change reduced the overall thrust capacity by around 15%, but was deemed acceptable with a balance piston. When operating with a high pressure-compressor, thrust position and thrust bearing RTDs will be evaluated closely during initial start-up to ensure proper thrust balance.

Figure 15 shows the final cross-section of the compressor. The compressor was designed as a back-to-back concept accommodating both the main and bypass compressor in the sCO_2 RCBC. However, for the initial testing, only the main compressor impeller was implemented and the two recompressor impellers are represented as simple disks to capture the impact on rotordynamic behavior. The barrel design uses a modular bundle that can be installed and removed from the case as an assembly to simplify installation and maintenance. The bundle utilizes non-split diaphragms made possible with the modular rotor construction with a central tie-bolt. The main compressor diaphragm must support 2,466 psia (17.0 MPa) pressure differential and contain the variable IGVs. Due to the relative small diameter of the main impeller, the hub diameter at the impeller is smaller than the dry gas seal diameter, which is driven by the journal bearing, coupling, and inboard thrust bearing arrangement, making a traditional shrunk-on impeller impossible without unacceptably poor rotordynamic behavior. The modular assembly solves this design challenge while maximizing rotor diameter along the shaft. In order to improve the structural integrity of this high-density impeller, a 5-axis electrode discharge machining (EDM) was utilized in its manufacturing followed by extrude-honing to improve surface finish resulting in a single-piece part (no welding or brazing for the cover).

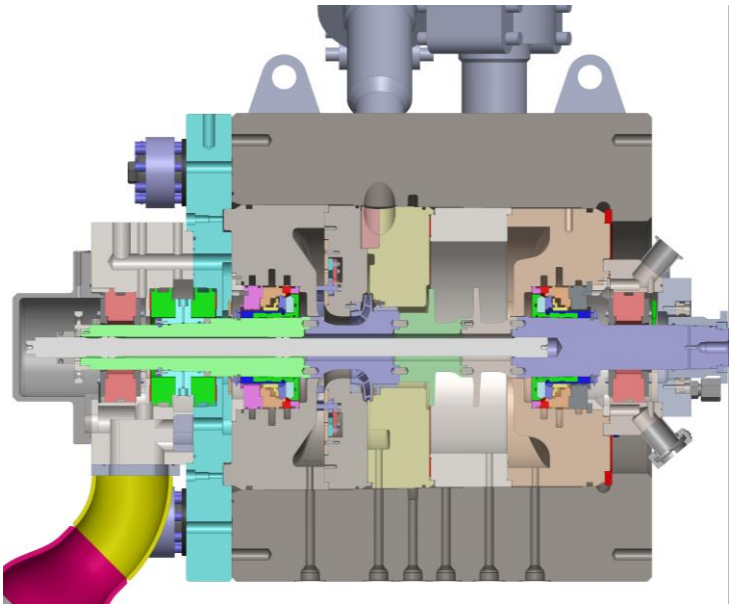

Figure 15 - Apollo Compressor Cross-section

COMPRESSOR DESIGN

For this design, it is important to note that the focus is on a back-to-back compressor with both a main (single stage) and a bypass (two-stage) section in a single casing [17]. While this is meant for the RCBC for power applications, a back-to-back design like this could be used to increase flow capacity or package multiple stages of a CCS / EOR cycle.

Similar to all rotating machinery, but especially important when designing a compact and power dense centrifugal compressor, which is required for sCO_2 compression, it is important to balance and understand the goals of three main design disciplines: aerodynamics, rotordynamics, and mechanical design. Figure 16 shows some of the important goals of each discipline:

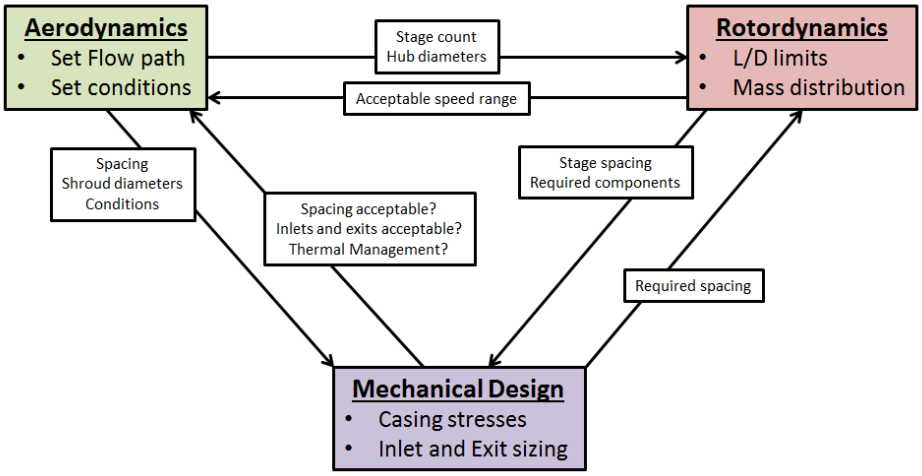

Figure 16 - Compressor Design Disciplines

Aerodynamics focuses on the flow path of the process fluid through the machine. This includes inlet and exit volutes, inlet guide vanes, compressor blades, and diffusers. In order to increase aerodynamic performance, the aero design will look to more stages, longer axial span, smaller hub diameters, and larger inlets.

Rotordynamics focuses on the overall stability of the shaft. This includes looking at bearing stiffness, damping coefficients from seals and dampers, and ensuring that the shaft has significant margin to lateral modes at operating speeds to prevent damage to the rotor and the rest of the machine. To improve rotordynamic stability, rotor design will look to decrease the axial span, increase the hub diameters, and utilize damping features like hole-pattern damper seals.

Mechanical design focuses on the stresses in the casing and the shaft. This includes hoop stresses in the casing, blade and hub stresses in the shaft due to rotation and temperature, fatigue and creep life, and the overall packaging of necessary components and features. To

reduce stresses and improve the mechanical life of the machine, mechanical design leads to smaller inlets, longer axial stages, fewer stages, and smaller case diameters.

As can be seen by the various design goals of each discipline, there are contradictions. Depending on the goal configuration of the system, certain design goals can be met more than others. For a system in which the main compressor and bypass compressor are not in a single casing, more stages could be designed for each compressor and the hub diameters could be decreased to improve the overall efficiency of each compressor. This would also mean fewer components to package and shorter axial span since only one compressor would have to be contained. From a design perspective, this is a much simpler solution; however, from an overall cost and foot print, this is not ideal. By having two separate compressor systems, this means two skids, at least two gearboxes, two motors, and an additional high-pressure casing. All of this leads to more piping, a larger required footprint, and will end up leading to higher costs and performance loss due to power required for additional bearings, gearboxes, and motors.

By combining the main and bypass compressor into a single casing and directly coupling it to the turbine, the overall footprint and cost of the system is decreased. The complexity of the compressor design is increased significantly, and the balance of the three disciplines will have to be considered even more. For this compressor design, the main goals will be:

1) Fewer compressor stages to reduce the overall axial span
2) Larger hub diameters that will meet bearing span to diameter goals set by rotordynamics and aerodynamics
3) Pushing the rotordynamic limits by balancing stage count, axial span, and key diameters to meet the overall design goals set by the cycle

To begin the layout and design, it is important to know the necessary components inside the compressor. As with the 14 MW turbine designed under the Sunshot project, this compressor will run on integral squeeze film damper tilting pad bearing [15]. Because sCO_2 is the operating fluid, dry gas seals will be required to limit CO_2 losses. With the challenges of installing both compressors and actuated IGVs, it is important to use as much existing technology as possible to limit the risks. Thrust bearings and a balance piston will also be required to manage any axial loading acting on the rotor. While the nominal design will have balanced thrust between the two compressors, off design cases will be looked at to ensure that the thrust bearings will not be overloaded. This compressor will also require a coupling on the drive end and a balance drum on the opposite end. Figure 17 shows an example of a compressor layout:

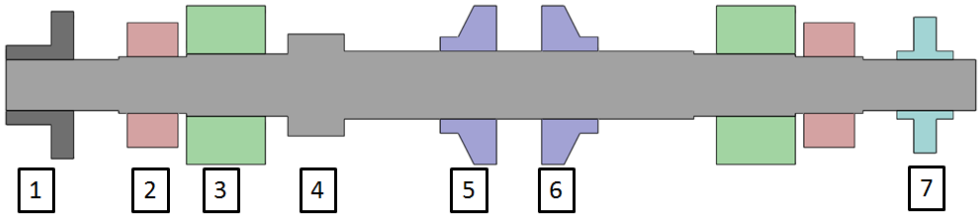

Figure 17 - Initial Apollo Rotor Layout with Necessary Components

Locations for internal components:

1) Coupling
2) Journal bearings
3) Dry gas seals (DGS)
4) Balance Piston
5) Main Compressor / Bypass Compressor
6) Bypass Compressor / Main Compressor
7) Thrust Collar

This compressor will be designed according to API 617 and ASME Boiler and Pressure Vessel Code Section VIII Division II (ASME VIII-2). API 617 covers many of the critical components on the shaft and stators and lists out the required analysis and studies to use for rotordynamics, mechanical design, and manufacturing. ASME VIII-2 is utilized to look at the pressure containment of the casing. Since the temperatures for this compressor are not pushing material limits, materials recommended by both of these codes will be used to limit additional design risk. It is important to note, while not discussed in detail in this tutorial, that material compatibility with CO_2 is important to consider in regards to casing, rotors, seals, and bearings, especially if there is a possibility of water in the system. While more expensive, Austenitic and Martensitic stainless steels are safe options, but do have other challenges that have to be considered (lower strength, differential thermal growth, galling).

Component sizing begins with the furthest outboard component, which is the coupling on the drive end of the shaft, which will see the smallest diameter and also peak stresses from torque. For assembly, it is important that the diameters step up from the coupling diameter to allow for ease of installation and also prevent damaging of critical surfaces. As mentioned before, one of the big advantages of sCO_2

is the compact flow design. With its high-density, the airfoils on the impellers can be made relatively small and reduce the overall size of the machine. However, the power consumed is high for the small frame size, which means the shaft has to be able to handle the torque. Depending on the source of the torque, certain safety factors are required. If this were a motor driven compressor (which would be required for CCS and EOR), it would need to account for start-up transients that could lead to torques 5-10X greater than the max continuous torque of the compressor [21]**.** Since this compressor design is turbine driven, the transient torsional stresses will be limited and safety factors can be limited to 5X to yield. From coupling vendor's data, Figure 18 shows shaft speed and power vs shaft diameter:

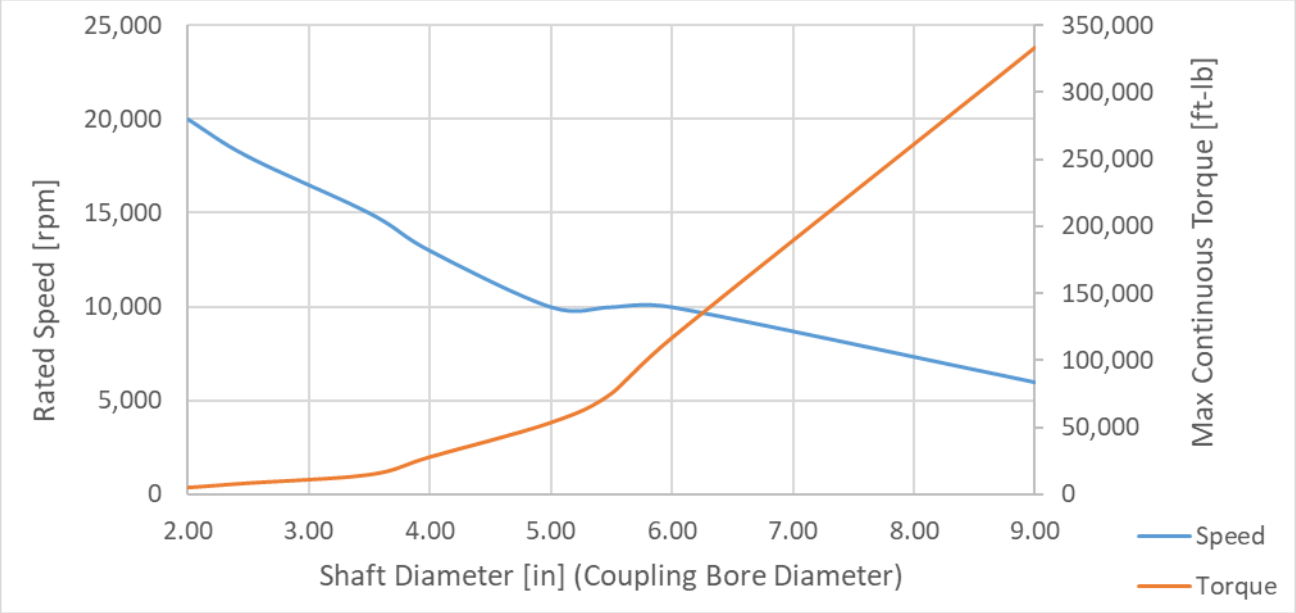

Figure 18 - Coupling Speed and Power Ratings [21] to Highlight Impact of Shaft Diameter for Sizing of Compressor Shaft Ends

For this compressor, the design power is at 6,570 hp (4.9 MW) at 28,350 rpm, 5% above operating speed of 27,000 rpm [15]. This limits the max coupling size to around 2.25 in (57.2 mm), size 6135/8135 high performance disc coupling. A coupling of this size has a max continuous torque 42,000 in-lb (4,745 N-m), a max peak torque of 52,000 in-lb (5,875 N-m), and a max short circuit torque of 67,000 in-lb (7,570 N-m). The torque from this compressor:

$$T = 63{,}025\frac{P}{w} = 63{,}025\frac{6570}{27000} = 15{,}336 \quad (1)$$

T = Torque, in-lb
P = Power, hp
w = Speed, rpm

$$\tau = \frac{Tr}{J} = \frac{15336\ x\ 1.125}{2.52} = 6{,}857\ psi \quad (2)$$

τ = Shear Stress, psi
r = radius, in
J= Polar moment of inertia, in^4

$$J = \frac{\pi r^4}{2} = 2.52\ in^4 \quad (3)$$

The peak shear stress from torque is far below standard shaft material, AISI 4140, which has a yield stress of 95 ksi (655 MPa). In order to meet the 5X safety factor to yield, the minimum shaft diameter is 1.6" (40.6 mm) based on torque and maximum of 2.25" (57.1 mm) based on coupling speed limits. Due to torsional requirements for the turbine, a 2.25" coupling will be used to allow for adequate safety factor.

With a 2.25" coupling, the minimum bearing diameter is 2.5" (63.5 mm). This is due to a required step up in diameter to allow for installation of the bearing. Without this step, the bearing could slide across the coupling surface and be damaged. In most cases, a minimum diameter step of 1/4" (6.4 mm) is required. With the small size of flow path and shaft, the bearings will not be seeing high loads due to the mass of the rotor.

After the coupling and bearings have been sized, the next step involves determining the hub diameter of the impellers. Since the impellers are in the middle of the shaft, the hub diameter will be critical in determining the max bearing span of the rotor. For compressors like this, a max length to bearing diameter ratio of 10 is recommended for conceptual design before a full rotordynamic analysis can be completed.

The minimum and maximum hub diameters are limited based on torsional and rotating stress requirements respectively. Earlier, it was determined that the minimum solid shaft diameter is 1.6". If a built up shaft is chosen, a tie bolt is required to hold all of the joints

together. The tie bolts diameter will be chosen based on pressure loads and rotational moments from the impellers. A larger tie bolt will lead to larger hub diameters to maintain minimum cross sectional areas.

For rotating stresses, the limit will be 50% of yield at the inner diameter. It is important to note that this is only considering the peak stress in the hub. Finite element analysis (FEA) will be required when looking at peak stresses in the blade geometry. Localized peak stresses can be higher than yield. The peak stress at the ID of the impellers is:

$$\sigma = \frac{3+v}{8}\rho\omega^2\left[r^2 + 2R^2 - \frac{1+3v}{3+v}r^2\right] \quad (4)$$

σ is peak stress at the smallest diameter, psi
v is poisson's ratio
ρ is material density, lbm/in^3
ω is rotating speed, rps
r is the inner diameter, in
R is the outer diameter, in

At 450 rps (27,000 rpm), the max diameter is 6.26" (159 mm) for a solid shaft and 6.18" (157 mm) for a shaft with a 2" (50.8 mm) tie bolt. This outer diameter is an initial assumption on the max diameter of any impeller, balance piston, and thrust collar. Since the impellers will have the blade geometry, their diameters can be larger. This is a hard limit for balance pistons and thrust collars since their geometry is a solid cylinder.

Aerodynamic detailed design will determine an appropriate hub diameter to impeller exit diameter ratio for peak performance. If this ratio is 0.5, the hub diameter would be around 3" (76.2 mm) which would allow for a bearing span of 30" (762 mm), see Figure 19:

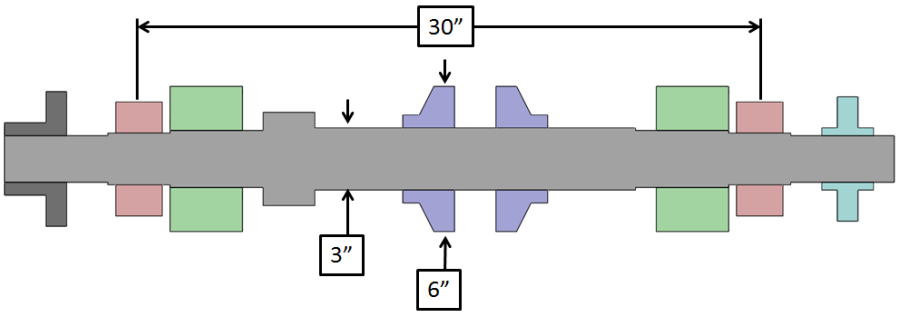

Figure 19 - Initial Apollo Rotor Bearing Span and Hub Diameters

Depending on the final tie bolt size, the minimum hub diameter will be determined by the torsional requirements. In Equation [2], replace J with:

$$J = \frac{\pi}{2}(R^2 - r^2) \quad (5)$$

J = Polar Moment of Inertia, in^4

Table 1 – Tie Bolt Diameters vs Minimum Shaft Outer Diameter

Tie Bolt Diameter	Min. Hub Diameter	Bearing Span
in	in	in
0.50	1.61	16.1
0.75	1.65	16.5
1.00	1.72	17.2
1.25	1.82	18.2
1.50	1.97	19.7
1.75	2.15	21.5
2.00	2.34	23.4

A larger tie bolt means higher clamp load, which is good for keeping joints in contact. This also leads to longer bearing span, but it does limit the minimum hub diameter. Torsional requirements set the minimum shaft diameter and rotational stresses set the maximum diameter. Within these bearing spans of 16" to 30", the optimal design and layout for the Apollo compressor will be determined.

With minimum and maximum spans based on required shaft sizes known, the next step is to determine required axial spacing based on stator components. Stator components of concern are the pressure containing end caps, diaphragms, division wall, and inlet and exit

plenums for both compressors. End caps are sized to ensure that they can contain the full design pressure of the compressor. To allow for off design performance, compressor casings are designed to contain 125% of max operating pressure (3,950 psia [27.2 MPa]) per API 617. For the case of the Apollo compressor this means the case and end caps will be designed to meet ASME Section VIII-2 at 400°F (204°C) and 4,800 psi (33.1 MPa). For initial sizing and axial spacing requirements, the end caps can be designed based on simple hand calculations show in Figure 20 and Table 2:

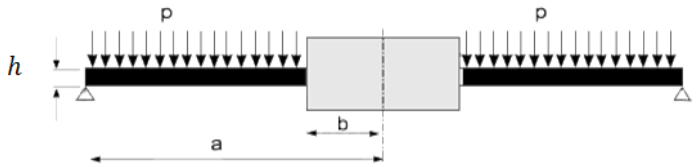

Figure 20- Simply Supported Plate [22]

$$\sigma_{max} = \frac{k_1 P a^2}{h^2} \quad (6)$$

$$w_{max} = \frac{k_2 P a^4}{E h^3} \quad (7)$$

σ_{max} is the peak stress in the diaphragm, psi
w_{max} is the max displacement at the ID of the diaphragm, in
a is the outer diameter
b is the inner diameter, in
P is the pressure, psi
h is the required thickness
E is modulus of elasticity, psi

Table 2 - K Factors for Diaphragm Thickness Calculations [22]

a/b	Simply Supported		Fixed Support	
	k1	k2	k1	k2
1.25	0.592	0.184	0.105	0.002
1.50	0.976	0.414	0.259	0.014
2.00	1.440	0.664	0.480	0.058
3.00	1.880	0.824	0.657	0.130
4.00	2.080	0.830	0.710	0.162
5.00	2.190	0.813	0.730	0.175

σ_{max} is based on the allowable stress of the material at design temperature as specified by ASME Section II Part D. w_{max} is limited based on the maximum displacement allowed in the diffuser of the compressor. The goal is to keep this displacement at <10% of the diffuser width to minimize aerodynamic differences at low and high pressure. End caps will usually be sized with stress as the limiting factor while diaphragms will be sized with displacement as the limiting factor. The pressure acting on the diaphragm is the pressure difference between inlet and exit of each compressor stage.

Analyzing the diaphragms and end caps based on the simply supported plate is a conservative approach. There are similar K factors for a fixed supported plate which are not conservative. Based on how the diaphragms are supported by adjacent parts, the actual displacement and stresses will fall in between simply supported and fixed support plates. Before a design can be finalized, the diaphragms and end caps must be confirmed with FEA according to ASME Section VIII-2. See Figure 21 for an example of simply supported plate. Final geometry will require supporting features and rough contacts to accurately simulate how each diaphragm and housing is supported. End caps will be affected greatly by how the pressure is contained, whether it is bolts or shear faces.

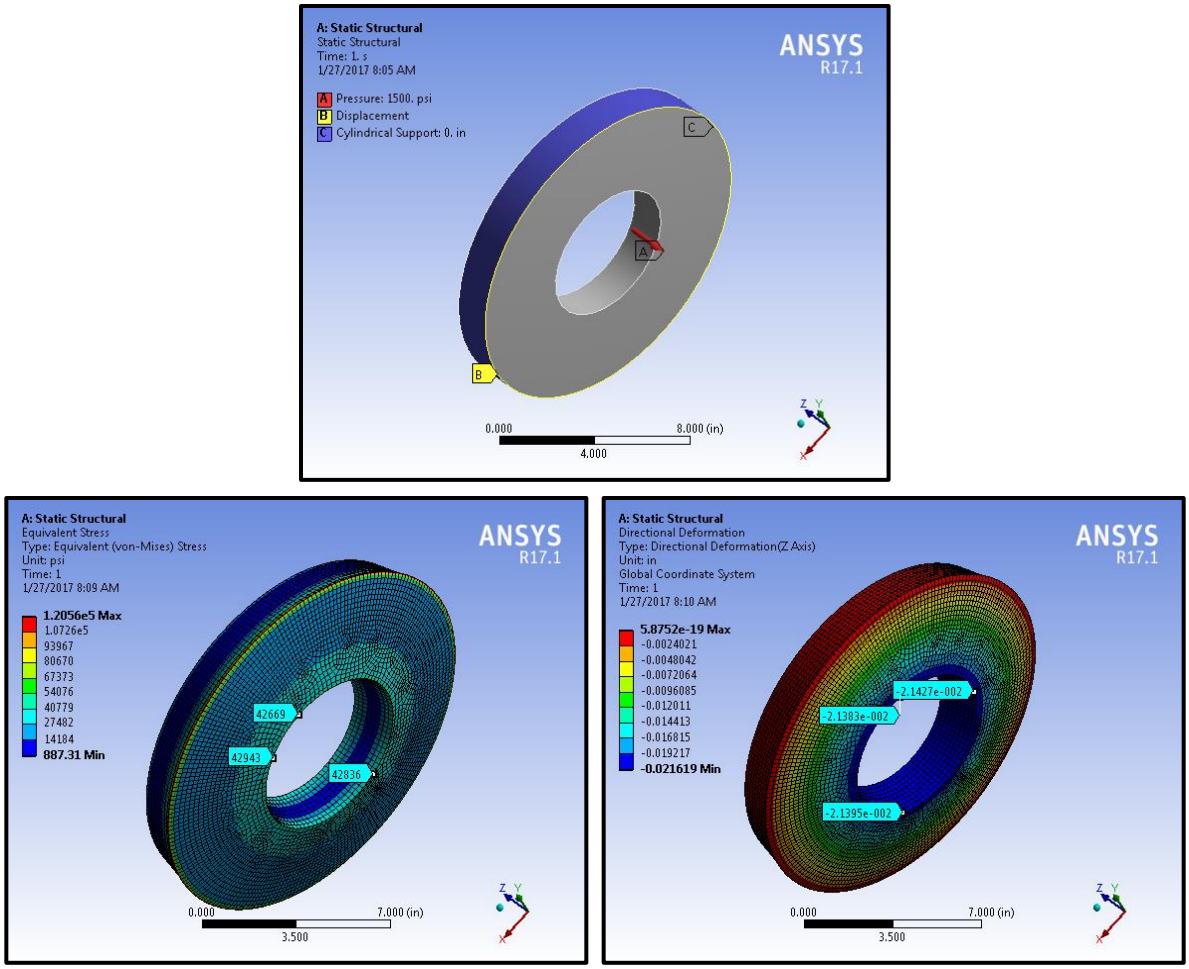

Figure 21 - Example FEA of Simply Supported Plate

Based on these equations, it is seen that as the outer diameter (a) is increased, the required thickness to maintain the required stress and displacement must also increase. This will limit the maximum outer diameter of the compressor bundle based on allowable axial span. Larger outer diameters allow for more radial space, including: shear rings, seals, bundle bolts, inlet and exit volutes, etc. With the high speeds and small diameters, axial space is limited for the internal components required. This leads to packaging constraints and design exceptions that have to be made. Figure 22 shows an example compressor layout with diaphragms, end caps, and outer casing:

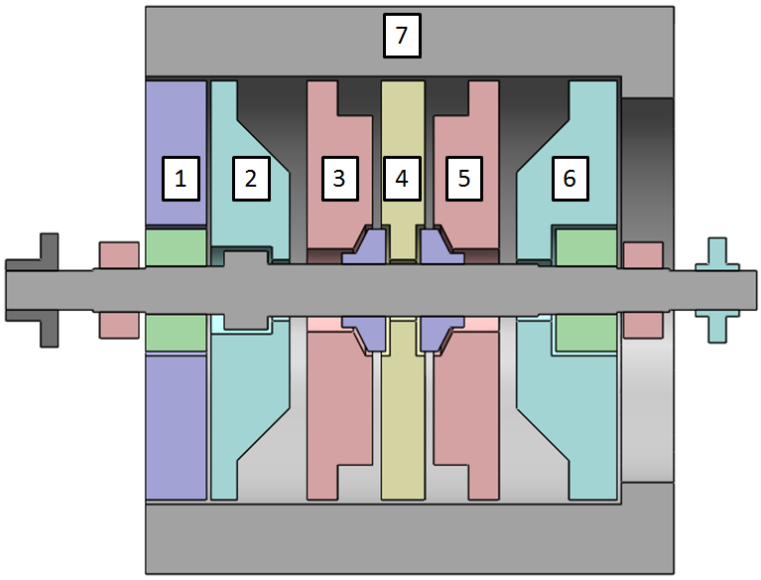

Figure 22 - Compressor Layout with Stator Components

Items (1) and (6) are the two end caps. These will be designed to contain the full design pressure of the compressor. The axial thickness at the OD is h in the stress and displacement calculation. Items (2) and (6) contain the inlet for the respective compressors. One houses the dry gas seal and the other houses the balance piston seal. This seal housing will require pressure tied to suction flow to allow for a pressure differential across the seal which will allow for damping and thrust control. Items (3) and (5) are the main and bypass compressor diaphragms. These will house the exit plenums and also the actuated IGV system. Item (4) is the division wall between both compressors. This will house a seal and should see zero pressure load. Item (7) is the outer casing. For a larger machine, this would be an axial split casing. For a smaller compressor like this, a sold barrel is preferred. The internal bundle containing the diaphragms and rotor should be able to be removed while the outer casing is installed on the operating skid.

For overall bearing span, the key features in addition to required diaphragm thicknesses will be in the inlet and exit flow paths. In the bundle, these flow paths will be scheduled volutes and plenums, but coming into the case will be standard piping connections, and to get to the bundle will require circular holes through the wall. The size of these holes is based on flow velocity limitations. ASME B31.1, Table IV-5.2 lists higher erosion rates for flows over 10 ft/s (3 m/s) for water and 150 ft/s (46 m/s) for steam. Based on density, sCO_2 is between water and steam, which leads to an average flow velocity of 80 ft/s (24 m/s) and can be used for initial sizing of inlet and exit piping. Lower velocities also reduce pressure losses. There is a balance between piping size, cost, and pressure loss. For longer lengths of pipe, the pressure loss is more significant, and for shorter lengths in the case of compressor inlet and exit nozzles, the pressure loss can be increased without affecting the overall pressure drop of the system significantly. Table 3 shows recommended flow path sizes for the inlet and exits of the main and bypass compressor.

Table 4 show axial spans for diaphragms and end caps based on the outer diameter:

Table 3 - Inlet and Exit Diameters Based on Maximum Flow Velocity

Section		Pressure		Temperature		Density	Mass Flow		Max Vel.	Min Dia.
		Mpa	psi	C	F	lbm/in^3	kg/s	lbm/s	ft/s	in
Main	Inlet	8.55	1,240	35	95	0.0224	70.3	155.0	80	3.03
	Exit	24.13	3,500	78	172	0.0247	70.3	155.0	80	2.88
Bypass	Inlet	8.69	1,260	88	190	0.0061	34.2	75.4	80	4.04
	Exit	23.99	3,479	194	381	0.0116	34.2	75.4	80	2.94
Main	Inlet	8.55	1,240	35	95	0.0224	70.3	155.0	150	2.21
	Exit	24.13	3,500	78	172	0.0247	70.3	155.0	150	2.11
Bypass	Inlet	8.69	1,260	88	190	0.0061	34.2	75.4	150	2.95
	Exit	23.99	3,479	194	381	0.0116	34.2	75.4	150	2.15

Table 4 - Diaphragm and End Cap Axial Span based on Outer Diameter of Bundle

OD	Material (Allowable Stress)			
	20 ksi	30 ksi	40 ksi	50 ksi
in				
10	11.13	9.15	7.98	7.21
12	14.92	12.27	10.69	9.77
14	18.54	15.25	13.29	12.27
16	22.06	18.15	15.81	14.72
18	25.54	21.01	18.36	17.16
20	29.01	23.87	21.00	19.63
22	32.49	26.73	23.67	22.13
24	35.89	29.53	26.33	24.63
26	39.06	32.14	28.85	26.99
28	41.67	34.29	30.96	28.96
30	43.15	35.50	32.09	29.98

Calculations for bundle span are based on the pressure difference between the following sections from Figure 22:

- inlet and exit on items (3) and (5)
- end caps, items (1) and (6), containing the full design pressure of the compressor casing
- division wall, item (5), containing the worst case pressure difference between main and bypass compressor
- balance piston diaphragm, item (2), which will see the pressure difference between inlet and exit

Bearing span must include axial spacing for the inlet and exit nozzles, the required thicknesses for all the diaphragms, axial allowance for the bearings, dry gas seals, and the balance piston. The bearing span is roughly equivalent to the bearings diameter, 2.5" (63.5 mm), and axial span for the balance piston diaphragm will be ignored since it can be included with the inlet or end cap. Dry gas seals are also contained within the end caps since this helps reduce space significantly. In a machine with more axial allowance, the dry gas seals could have their own housing, but that would require roughly 25% of max allowable axial span for this compressor.

If designed to 80 ft/s (24 m/s) flow velocity, the required span for flow paths is 12.9" (328 mm) and another 2.5" (63.5 mm) for the bearings, allows 14.6" (371 mm) for diaphragm axial span. This limits the maximum OD to around 16" (406 mm) with 50 ksi (345 MPa) allowable stress material. With a design velocity of 150 ft/s (46 m/s), the required flow path span is 9.4" (239 mm) and allows for 18.1" (460 mm) for diaphragm axial span. This allows for up to 18" (457 mm) OD with 50 ksi allowable material. Realistically, any pressure containing material will not have an allowable stress greater than 30 ksi (207 MPa), which limits this design to 16" bundle OD, a 30" (762 mm) bearing span, and a hub diameter of 3.00" (76.2 mm).

With the overall design envelope established, packaging of key internal components can begin. Current axial spacing already allows for bearings, dry gas seals, diaphragms, inlets, exits, and pressure containment. The last component, mainly for this design application, is the variable IGVs. As mentioned, earlier, variable IGVs will be required for the main and bypass compressor. Looking back at Figure 22, the variable IGVs will need to be packaged either in item (2) or (3) for the main compressor and item (5) or (6) for the bypass compressor.

Based on the diaphragm thickness calculations for the main and bypass compressor, the required thickness for each diaphragm is 3.00" (76.2 mm), items (2), (3), and (5), and the end cap is 3.88" (98.6 mm), item (6). Ideally, the actuator system could be placed in the end caps, where more room in available, but due to requirements for balance pistons, dry gas seals, and inlet plenums, the actual available space is much less. Balance pistons require flow capacity for the supply CO_2. Dry gas seals require porting for buffer air, venting, and supply CO_2. Inlet plenums require more flow area due to the lower pressures. This means the best location for actuator systems is in the compressor diaphragms between inlet and exit. The less space the actuator system requires, the more stages that can be added to increase compressor efficiency. If a single actuated vane system requires the full span of the diaphragm, this means each compressor can only have a single stage. If the span is half the required thickness, a 2nd stage could be packaged for each section.

There are two options for actuated inlet guide vanes: axial or radial as shown in Figure 23 and Figure 24 respectively:

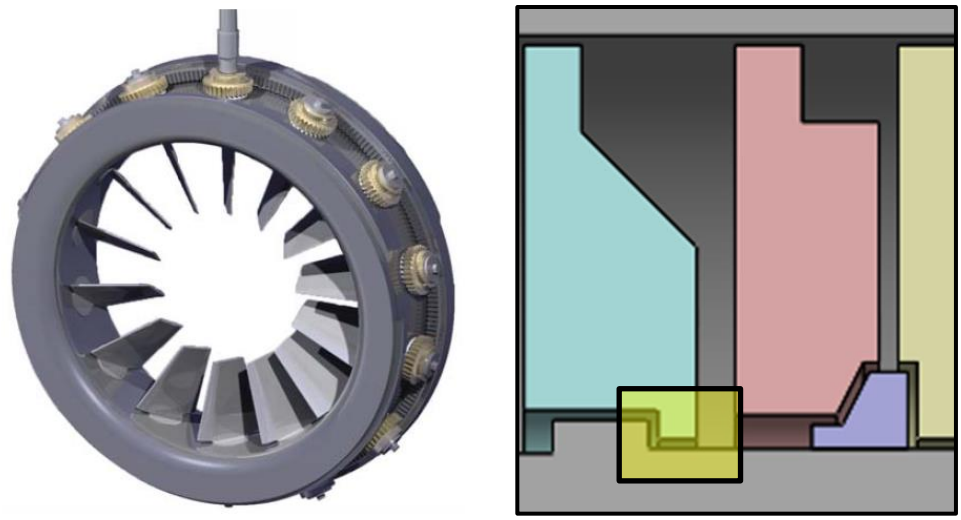

Figure 23 - Axial IGVs for a Radial Compressor [23]

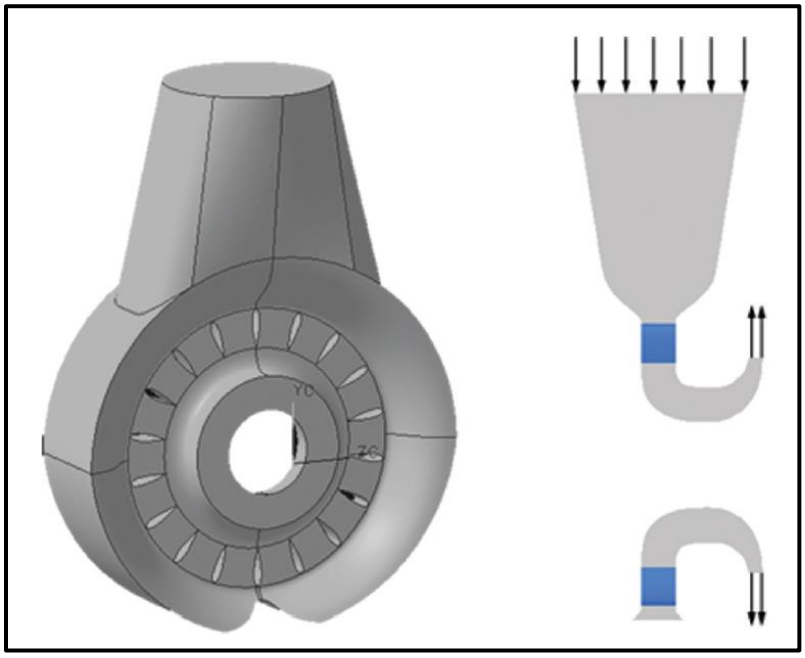

Figure 24 - Radial IGVs for a Radial Compressor [24]

Based on rotor layout, each IGV has its own advantage. For an overhung compressor where axial space on the stators at the end of the shaft doesn't affect rotor spans, axial IGVs would be used. They are also used in axial compressors where less axial space is required to contain an actuated IGV compared for a fixed IGV. When axial space is limited between the bearings, radial IGVs will be preferred. An actuated radial IGV system will require an external actuator that will penetrate through the pressure boundary of the case and connect with a pivot or gear system that can use a tangential load to rotate the IGVs radially. If a pivot system is use, each joint requires bearings. Operating in a CO_2 environment with limited space, the bearings will have to be unlubricated and will need to handle the loading from the actuator and the aerodynamic loading from the IGVs. The max load will be calculated based on the largest angle from the radial line to the center of the axis. Figure 25 shows the difference between setting angles on an IGV:

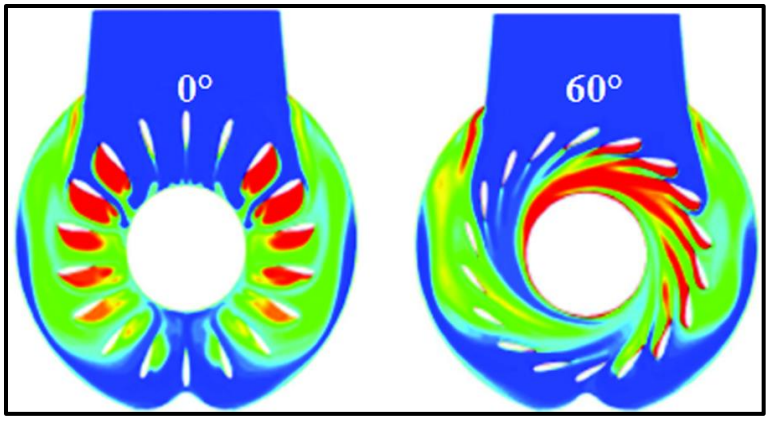

Figure 25 - Perfectly Radial IGVs vs Large Setting Angle IGVs [24]

Based on the above image, the aerodynamic force acting on the 60° case would produce a much larger load on the IGV. Figure 26 shows how these aerodynamic loads create a total load on the actuator:

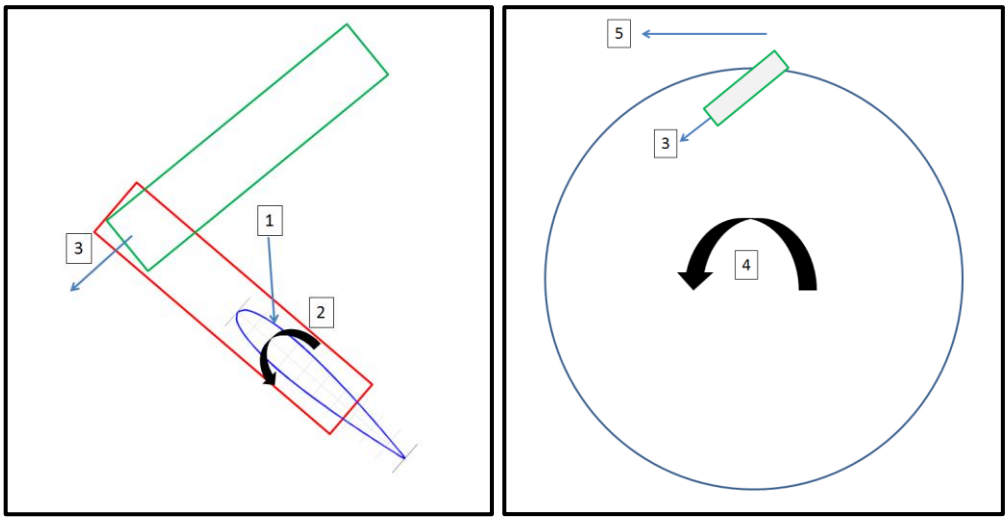

Figure 26 - Aerodynamic Loads acting on Actuated IGVs

The aerodynamic load (1) will create a torque (2) that will cause a load between the two pivot joints (3). This load is then transmitted to a rotating ring that will contain all of the pivot joints and create a torque (4) that will lead to a combined axial load on the actuator (5) from all of the IGVs. Since lubricated bearings will not work in this environment, non-lubricated bearings will be used and they will have a higher friction coefficient that leads to a larger load required by the actuator to not only maintain position but also rotate the IGVs during operation. This system will require one or two bearings at each joint based on the loads that are acting. One of the smallest bearings available is a ¼" shaft Teflon™ sleeve bearing. These bearings can only handle around 21 lbs. As the shaft diameter steps up, so does the length of the bearing. Length and diameter are key in determining how much axial and radial space is required to house the actuator. With a 3.00" (76.2 mm) axial span and max OD of 16" (406 mm), the actuator envelope must be smaller, while also allowing space for seals, bolts, and assembly/disassembly features. Figure 27 shows how the actuated system will affect the compressor diaphragm and how much space is required. This is assuming ¼" (6.4 mm) bearings:

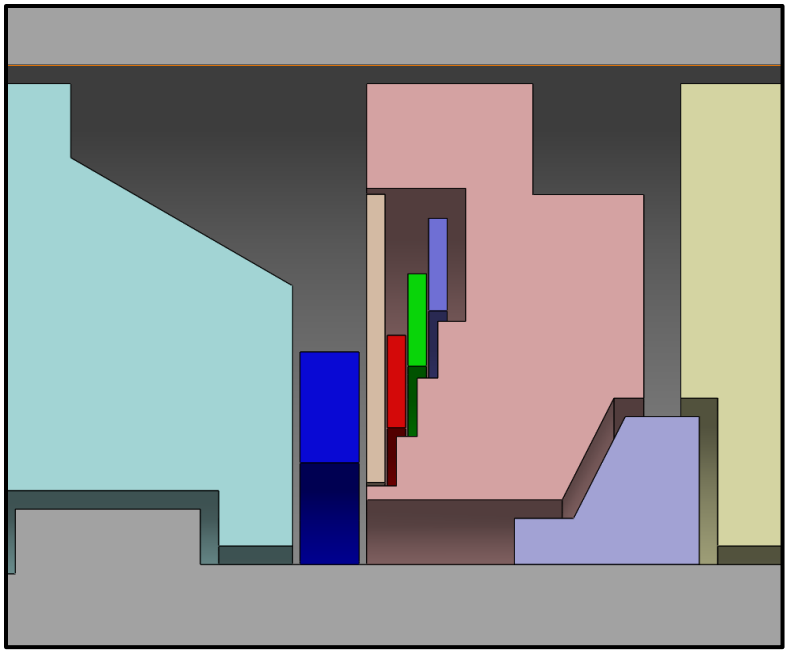

Figure 27 - Actuated IGV System Design Envelope in Compressor Diaphragm

ROTORDYNAMICS SUMMARY

As stated earlier, due to the high-density, the rotordynamics were a primary concern for this design. Figure 28 provides a geometry plot of the latest rotor model configuration being considered, which incorporates a tie-bolt, includes a thrust disc located within the bearing span, and squeeze film dampers in series with the bearing oil films. The total length of the rotor is 35.1" (859 mm), and the total mass is 88.0 lbm (39.9 kg). The model includes provisions for eye seals at each of the three impellers (current conservative preswirl assumption=0.15, although swirl brakes are to be incorporated in the final design), and a two-part hole pattern balance piston seal. Current bearing assumptions include: 5 shoe, load between pad, length/diameter of 0.6, and pivot offset of 50%. At present, pivot stiffness and pad deformation effects are not included, and an adiabatic solution is assumed. A bearing preload range of 0.25-0.37 has been specified, although results in this summary concentrate on the maximum preload (minimum clearance) condition.

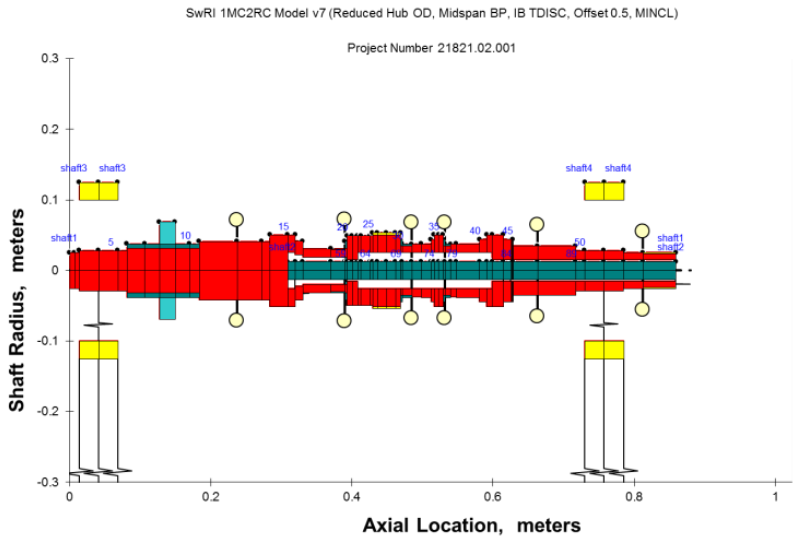

Figure 28 - Rotordynamic Model Geometry Plot

An undamped critical speed map is provided in Figure 29, with the first three mode shapes superimposed. The first undamped mode is dominated by motion near the mid-span of the rotor, and occurs at about 8,000 rpm. The second mode (occurring near 16,000 rpm) involves out-of-phase motion at the ends of the rotor, while the third mode (above 33,500 rpm) involves significant bending with in-phase motion at each end of the rotor, with some participation at the mid-span. The predicted frequencies of these modes would be expected to shift with the addition of bearing damping.

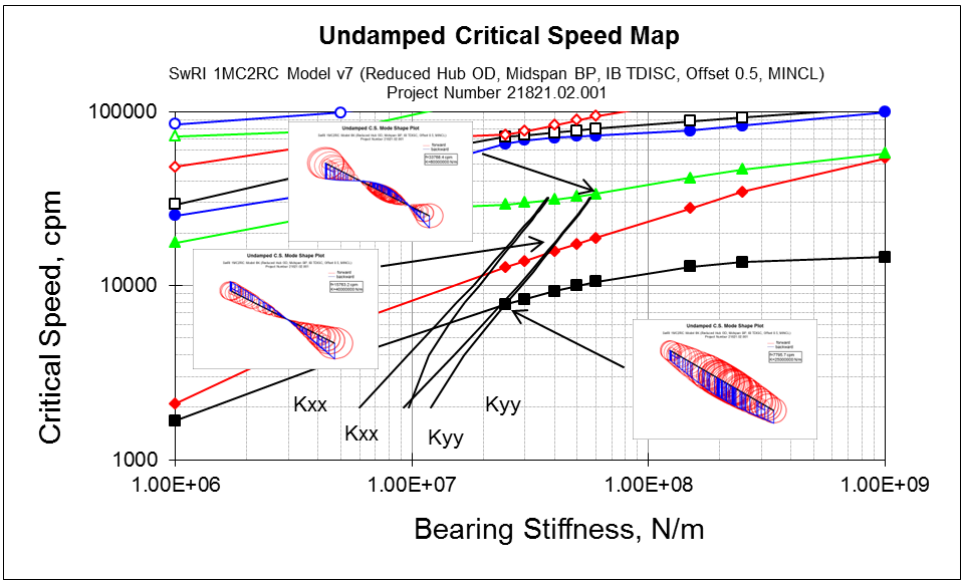

Figure 29 - Undamped Critical Speed Map and Representative Mode Shapes

Figure 30 provides a series of representative damped unbalance response plots for cases which include the effects of the rotor, bearing oil films, and squeeze film dampers. The plots in the left column involve unbalance located at the mid-span (center) of the rotor, while the center column plots are based on an ends out-of-phase unbalance configuration, and the right column plots are based on an ends in-phase unbalance case. These unbalance distributions are meant to excite the first three modes, respectively. In each case, a total of 4 times the specified API unbalance has been applied. The plots indicate a variety of very well damped response peaks associated with the first three modes. Figure 31 provides similar information for cases which include the stiffening and damping effects of the eye and hole pattern balance piston seals (assumed converging taper of 1 mil), based upon full running speed nominal inlet and exit pressures. All of the predicted response peaks in Figure 30 and Figure 31 meet API criteria due to the low amplification factors involved, although some response peaks are near or within the anticipated running speed range. Parameter studies conducted to date indicate that the frequencies of these response peaks are influenced by the bearing, squeeze film damper, and hole pattern seal characteristics. As these parameters are refined, further optimization of the predicted separation margins may be feasible.

Representative damped Eigenvalue plots are provided in Figure 32 and Figure 33 for configurations without and with seals, respectively. These plots indicate shapes that are consistent with the first mode. Both of these plots were prepared by including the full aerodynamic cross coupling specified by API. Figure 32, which indicates a log dec of 1.02 and includes only the effects of bearings, squeeze film dampers, and the applied aero cross coupling, is consistent with the intent of the API level 1 screening criteria. In this case, the calculated log dec exceeds 1.01, which meets API level 1 criterion, and illustrates an inherent benefit of the squeeze film dampers. Figure 33 is prepared for level 2 conditions, and includes the three eye seals with swirl brakes (which are slightly stabilizing), and the hole pattern balance pistons (which are quite stabilizing at the assumed converging taper of 3-5 mils (0.076-0.127 mm), along with the API aerodynamic cross coupling. These conditions result in a calculated log dec of about 3.9, which easily satisfies API level 2 criteria.

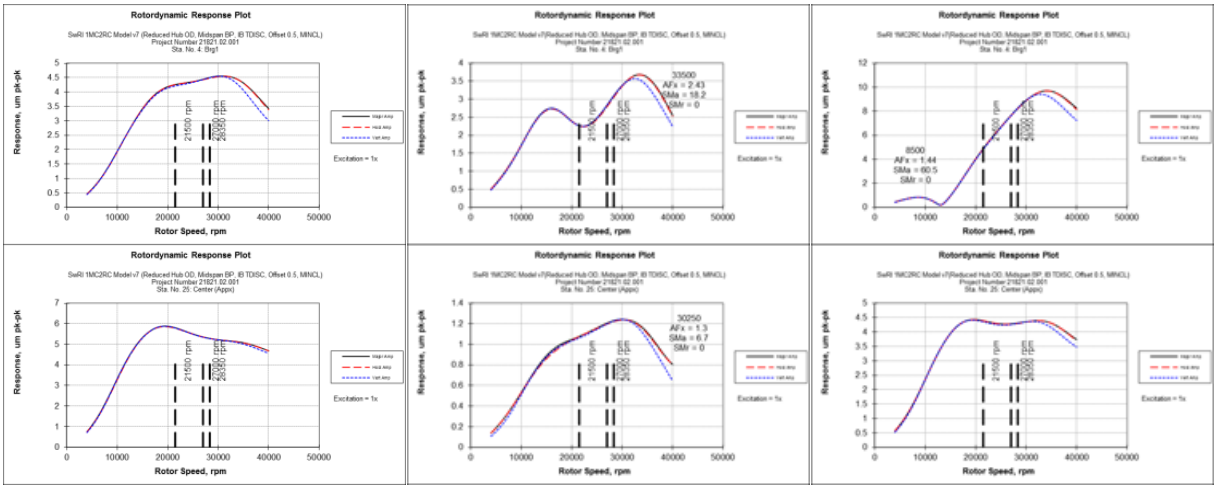

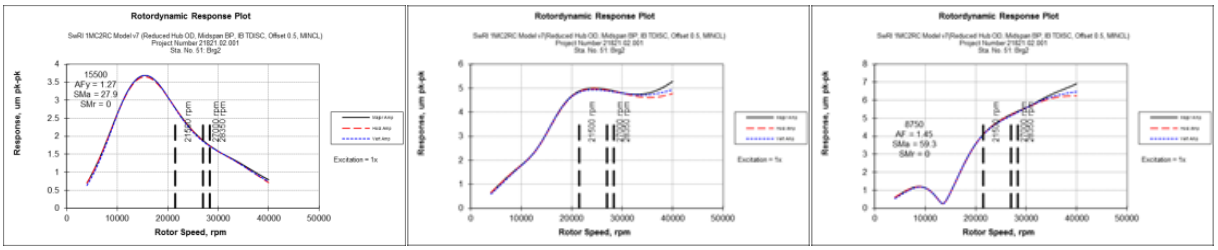

Figure 30 - Representative Unbalance Response Plots Without Seal Effects (Midspan, EOP, EIP)

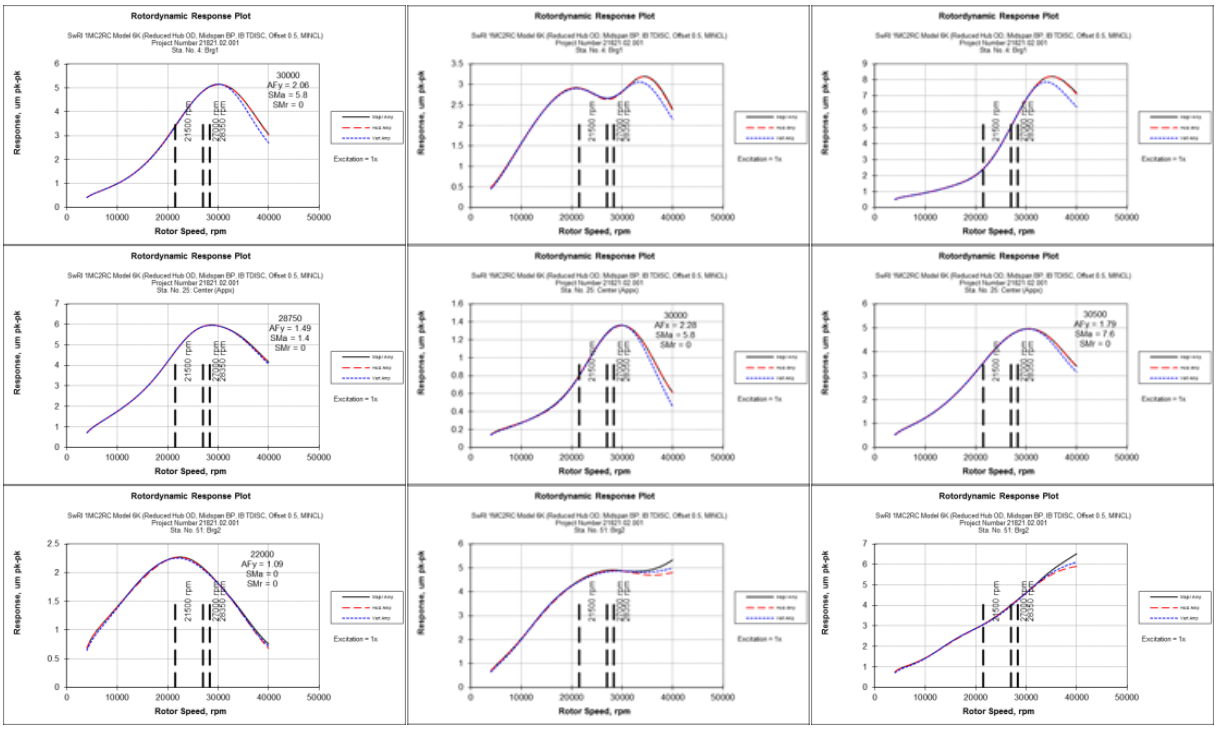

Figure 31 - Representative Unbalance Response Plots With Seal Effects (Midspan, EOP, EIP)

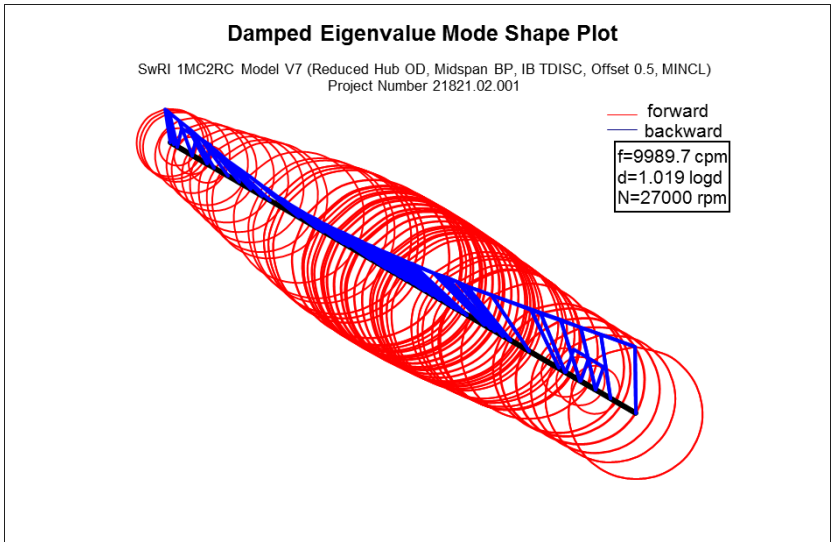

Figure 32 - Representative Damped Eigenvalue (Bearings/SQDs and Full API Aero Only)

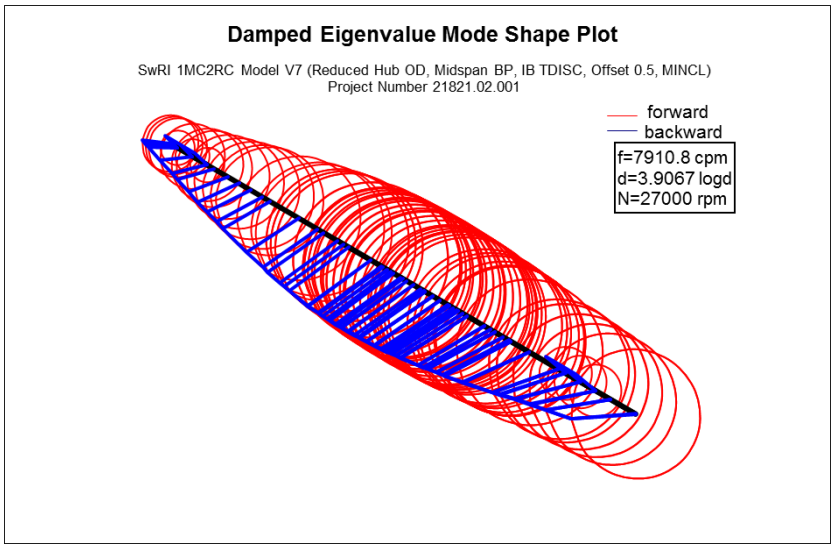

Figure 33 - Representative Damped Eigenvalue (With Stabilizing Seal Effects)

A stability map is provided in Figure 34 to illustrate the effects of variations in applied aerodynamic cross coupling on predicted log dec values. Two curves are presented, one of which includes seal effects, and one for the rotor and bearings (including the integral squeeze film dampers) only. These results, which are consistent with those shown in Figure 32 and Figure 33, further illustrate the stabilizing effect of the seals.

One well known feature of hole pattern seals is a sensitivity to taper (the difference between inlet and exit clearance). Figure 35 indicates that convergent tapers are generally stabilizing, but at low (below about 0.5 mil) convergent tapers and divergent tapers, the calculated log dec falls dramatically, accompanied by a rapid decrease in principal seal stiffness. To manage this effect, convergent operating tapers must be achieved, which can be influenced by division wall deformation (due to pressure effects), and part tolerances. In this case, a potential operating taper range is being considered in the 3-5 mil ((0.076-0.127 mm) convergence regime in order to take these factors into account. The figure also illustrates the generally stabilizing effects of the squeeze film dampers, which tend to increase the calculated log dec values in the anticipated operating taper range. An example hole pattern seal is shown in Figure 36.

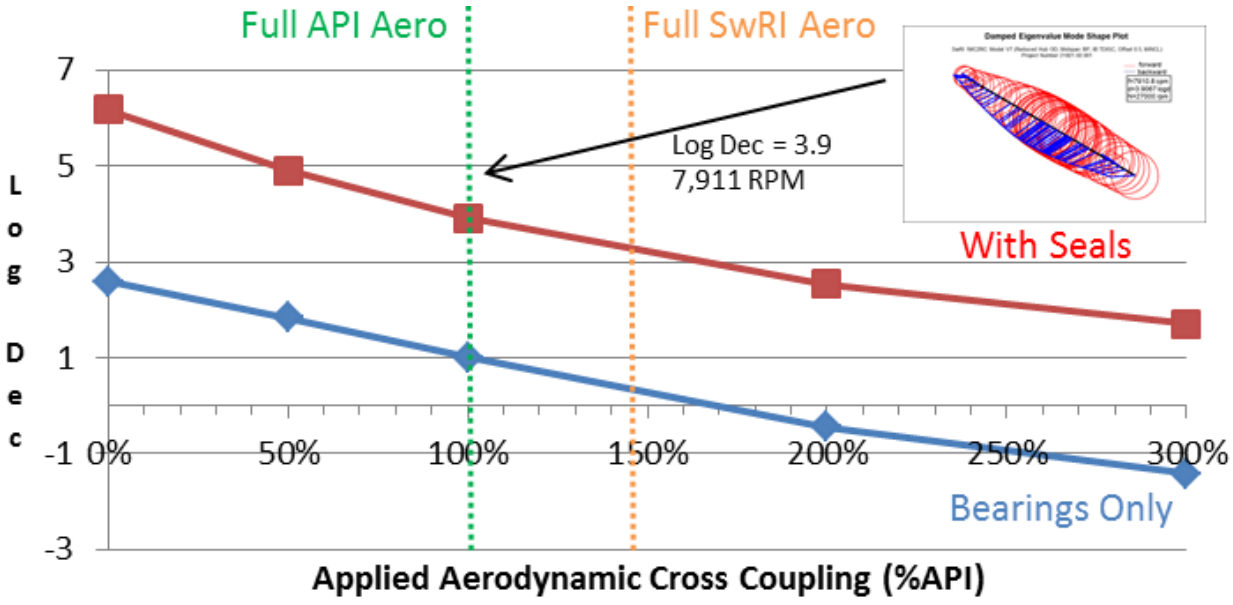

Figure 34 - Stability Map

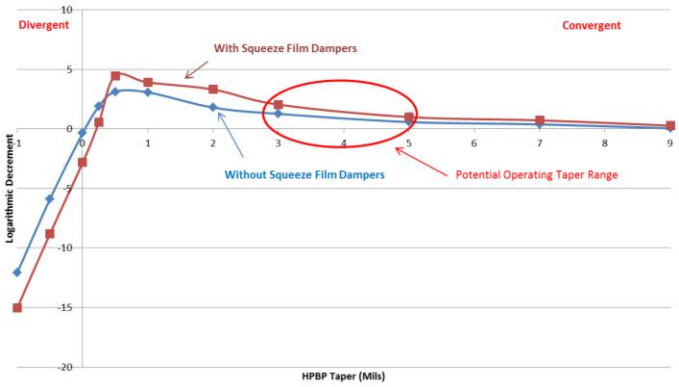

Figure 35 - Sensitivity of Stability to Hole Pattern Seal Taper and Squeeze Film Dampers

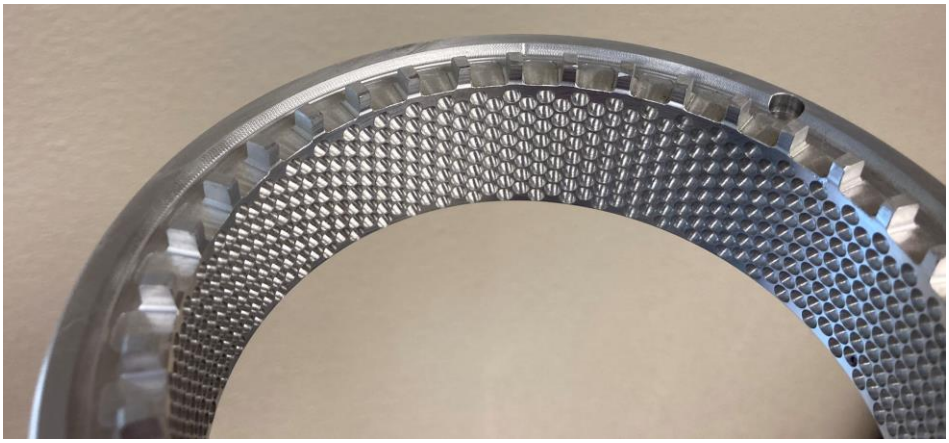

Figure 36 - Example Hole Pattern Damper Seal

Squeeze film dampers (SFDs) were implemented into the journal bearings to provide additional damping to smooth critical speeds and improve stability. However, SFDs one drawback is the low dynamic stiffness at low frequencies. Since the damper is in series with the stiffness and damping from the bearing oil film, the low frequency regimes is soft making the rotor susceptible to low frequency forcing functions as observed in the testing. Figure 37 shows the predicted non-synchronous dynamic stiffness of the journal bearing only (blue), squeeze film only (red), and the combined bearing and SFD coefficients in series (green) at 27,000 rpm. Near the frequency of 50 Hz (3000 cpm) where the vibration was observed (to be shown later), eliminating the squeeze film damper would increase the stiffness by about 7 times. The bearing manufacturer accommodated locking the damping by simply inserting dowel pins into the predrilled holes near the damper. Figure 38 shows the pins that were inserted to lock up the damper.

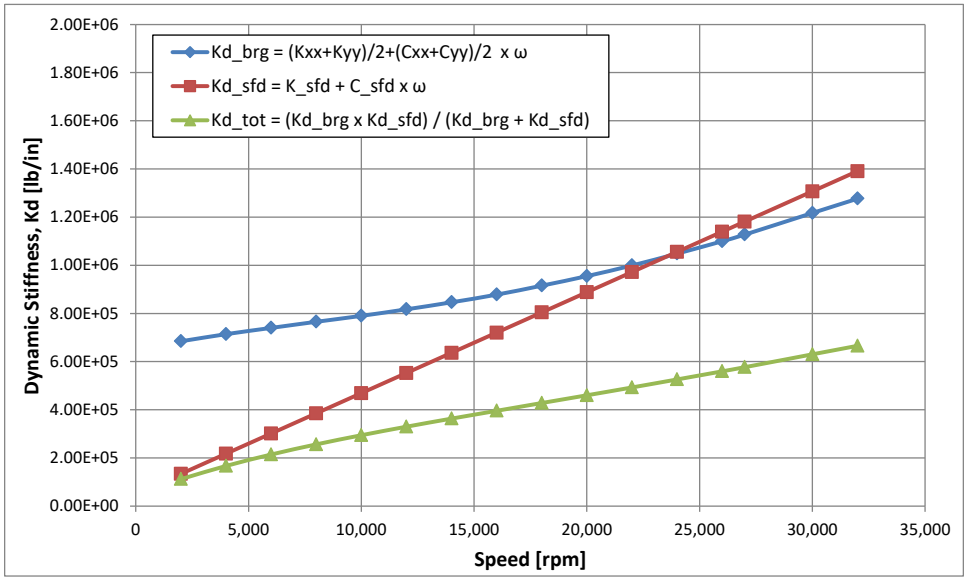

Figure 37 - Bearing Dynamic Stiffness Prediction

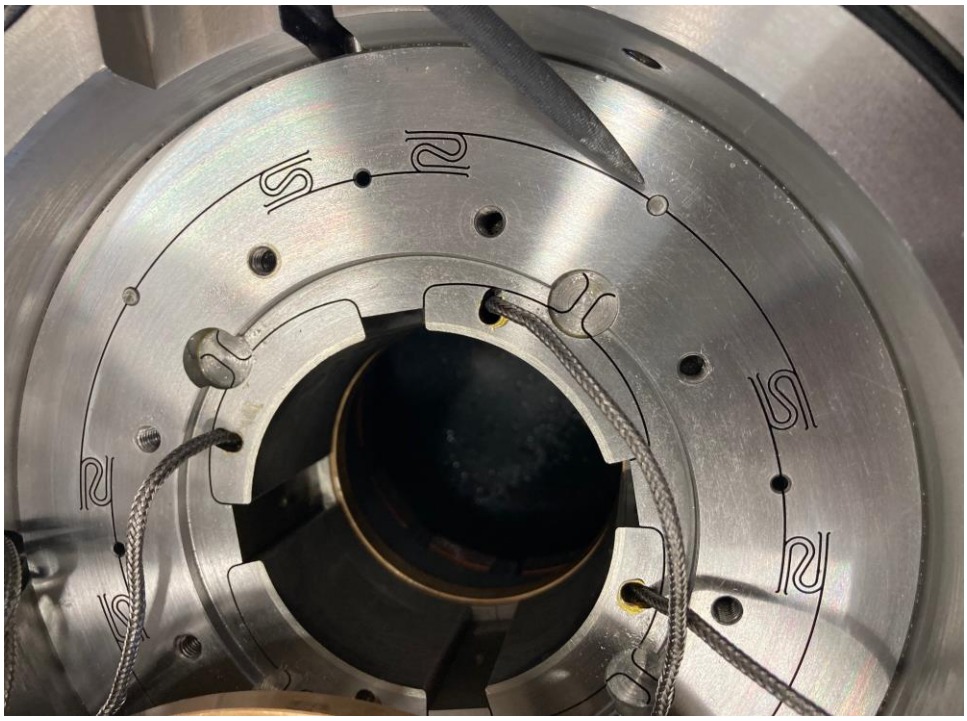

Figure 38 - Photo of Squeeze Film Damper Bearing with Locking Pins

The unbalance response and stability results of the current rotor configuration are considered to be generally satisfactory. For the final configuration without squeeze film dampers, the rotordynamic results were found to be satisfactory as well.

DATA VALIDATION

The following data below highlights some of the unique challenges with sCO_2. More detailed test data is shared in [26][16][27][28]. These papers summarize the mechanical performance of the compressor designed under this program and also some of the challenges associated with control, measurement, and rotordynamic performance. The design proved out the effective design of a sCO_2 centrifugal compressor and many of the operating aspects that have to be considered when designing a full sCO_2 compression system.

Figure 39 highlights performance data of this compressor at a few operating conditions, primarily 300 psia (2.0 MPa) at 95°F (35°C), 1240 psia (8.6 MPa) at 122°F (50°C), and 1240 psia at 95°F. Low-pressure data (300 psia) represents the preliminary and ideal gas compression performance of the Apollo compressor. This provides ideal gas compressor maps to compare real gas (high-pressure) performance. Based on polytropic head results, high-pressure operation at 122°F and low-pressure operation at the same IGV setting show similar performance maps. The main difference is the choked flow on the right side of the map. Large differences are seen as the flow is cooled at higher pressure. Green, yellow, and blue data all represent -30° IGV performance data. At lower temperature (lower speed of sound), the compressor chokes at lower flow rates, which is represented by the steep drop on the right side of the map. When designing sCO_2 centrifugal compressors, this choke point is important to consider as it will severely impact the maximum flow rate of the compressor.

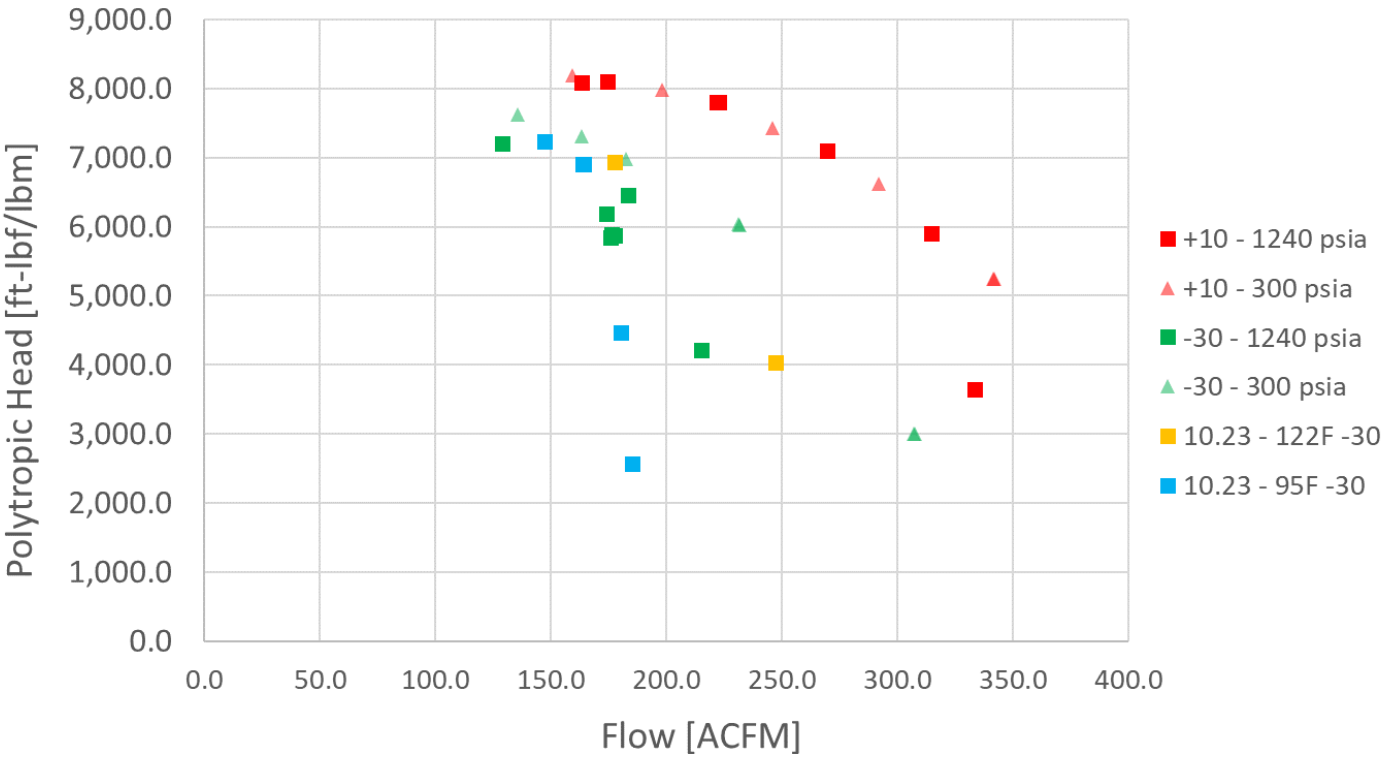

Figure 39 - Preliminary Compressor Maps (Polytropic Head Curve) at Low and High Pressure Suction Conditions

Figure 40 through Figure 44 highlights shaft vibrations at the bearings (mechanical performance) of the compressor at various operating conditions. It is important to note that all of this data represents performance with active squeeze film dampers. Figure 40 through Figure 42 show the impact of suction density on shaft vibrations. The peak vibrations scale linearly with suction density (at fixed speed and IGV set point). Figure 43 and Figure 44 highlight the difference between full-speed, low-density compression vs lower speed, high-density compression and the difference in sub-synchronous vibrations. These vibrations highlight the unique challenges of a high-speed sCO_2 centrifugal compressor. Special consideration is required for the overall mechanical and rotordynamic design of the machine.

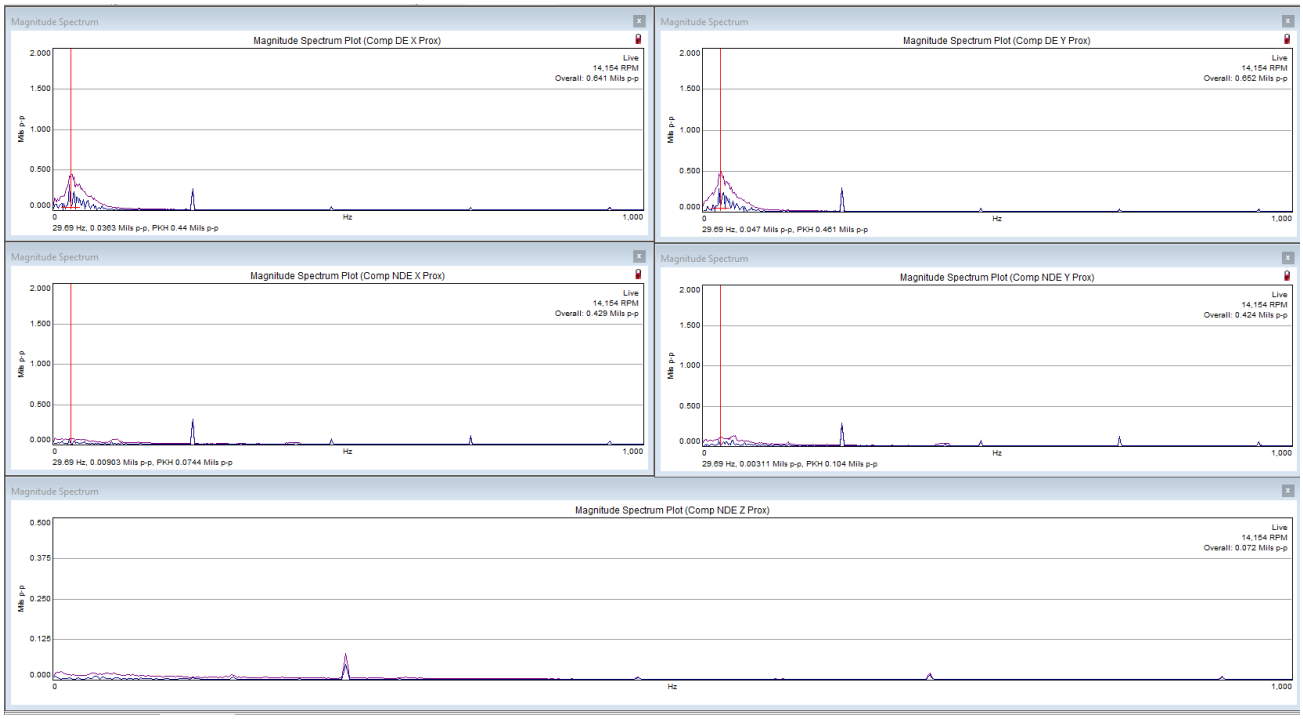

Figure 40 - Shaft Vibrations at 14,000 rpm with a Suction Density of 586 kg/m^3

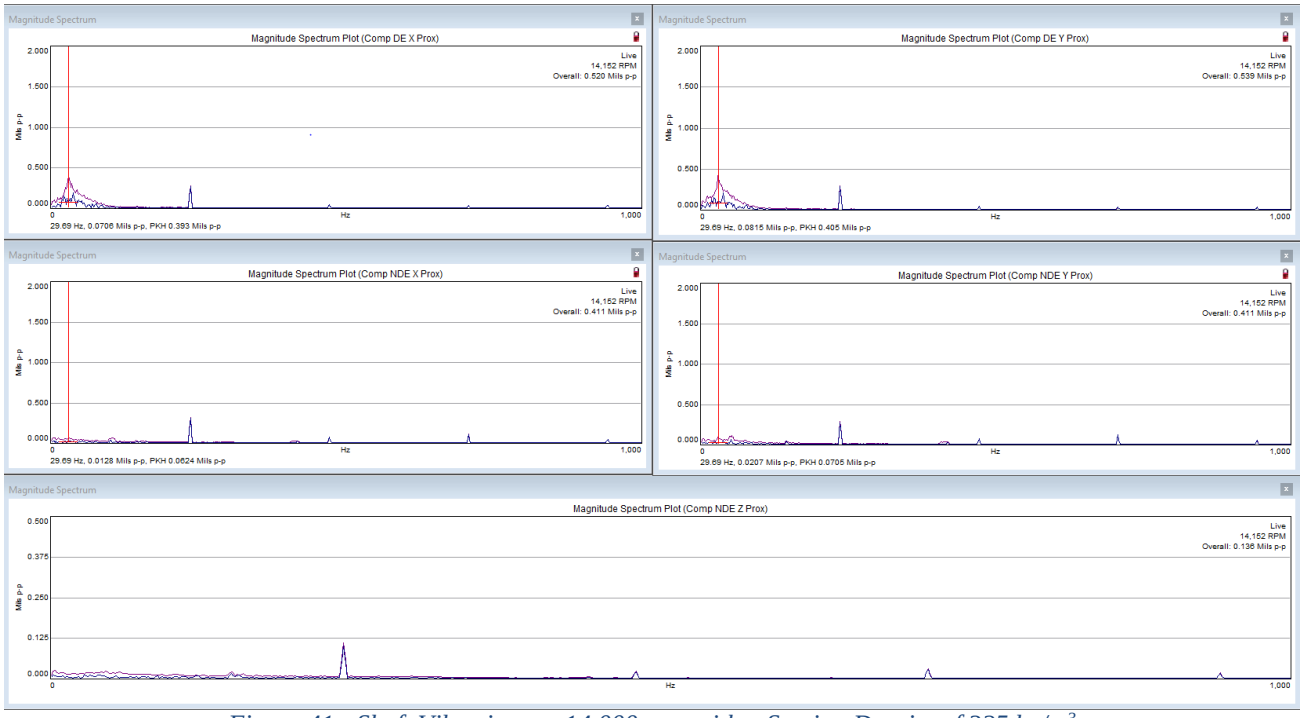

Figure 41 - Shaft Vibrations at 14,000 rpm with a Suction Density of 325 kg/m^3

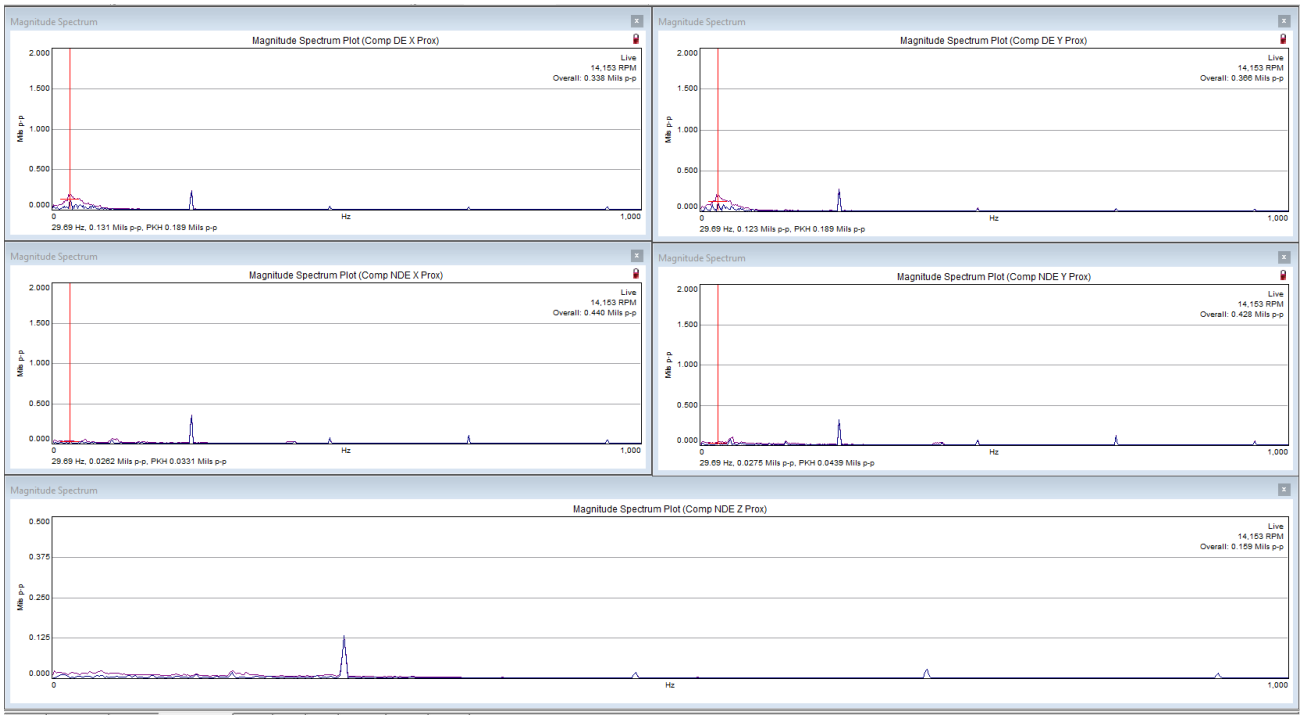

Figure 42 - Shaft Vibrations at 14,000 rpm with a Suction Density of 276 kg/m^3

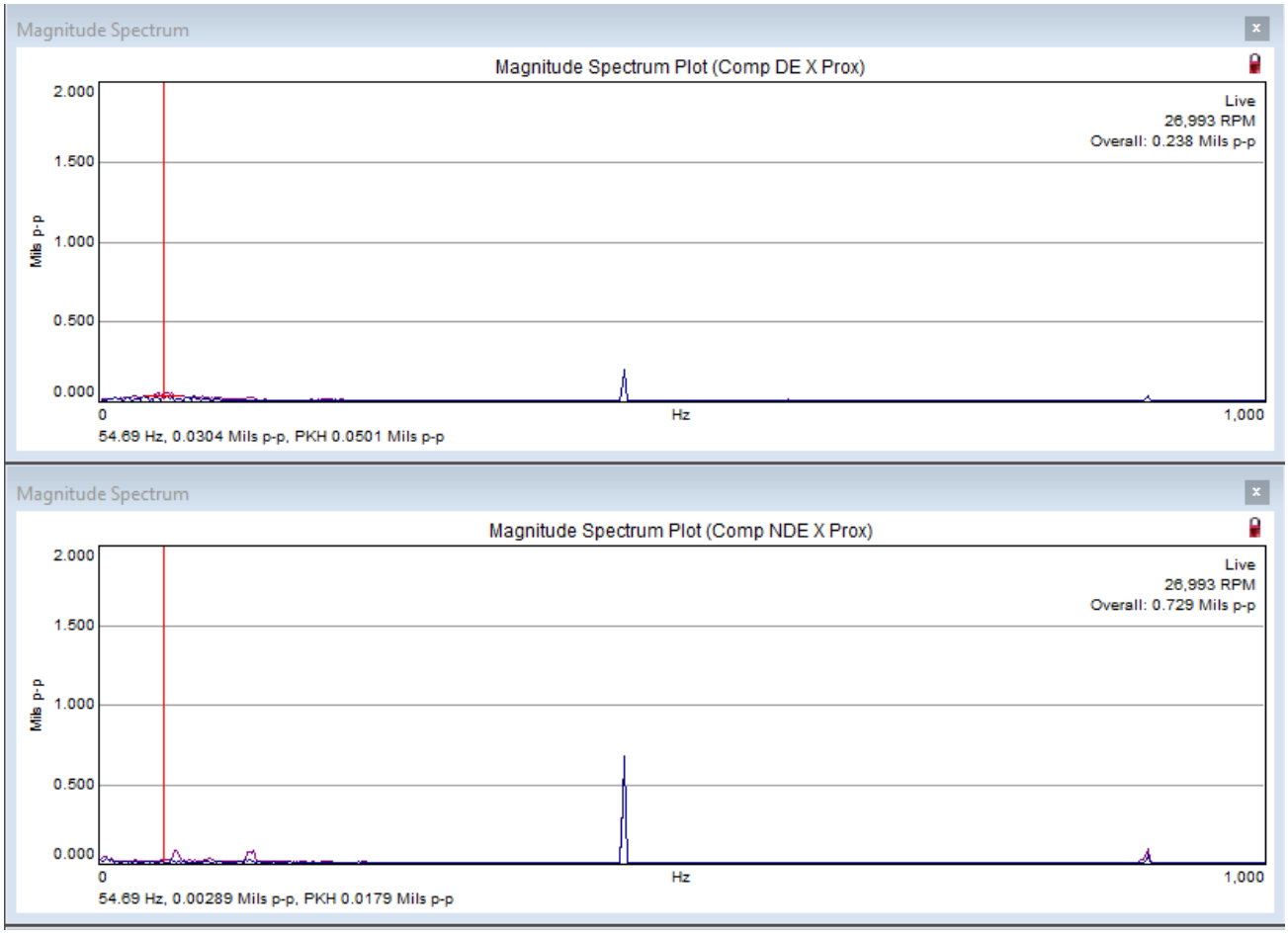

Figure 43 - Shaft Vibrations at 27,000 rpm at 2.0 MPa Suction

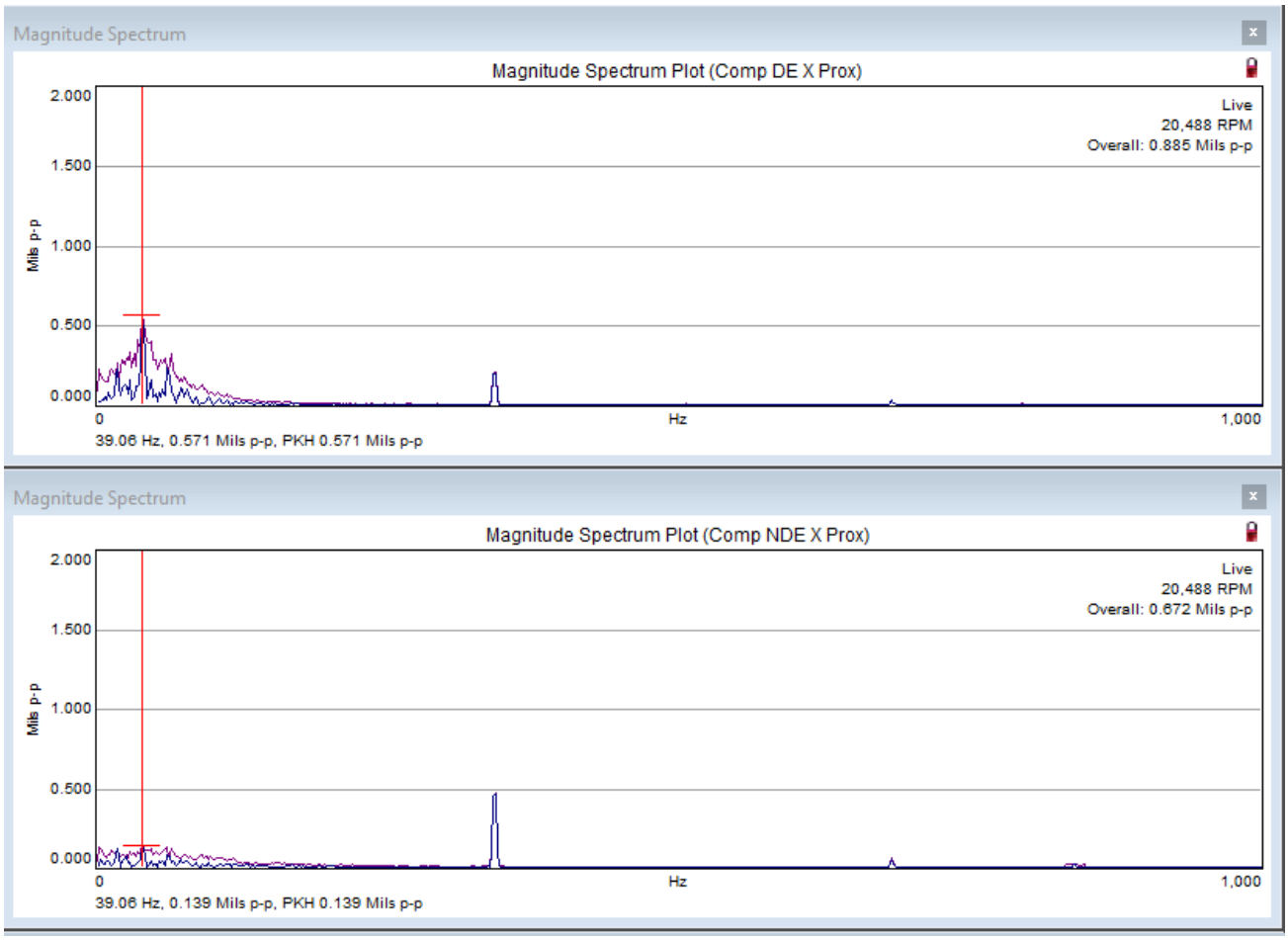

Figure 44 - Shaft Vibrations at 20,500 rpm at 8.5 MPa Suction

CONCLUSIONS

Design, development, and testing proved that a high-speed, high-efficiency sCO_2 centrifugal compressor is achievable. The program referenced throughout this tutorial provides a baseline for the development of future compression systems to improve CO_2 systems ranging from power cycles to downhole injection. Due to high-pressure and high-density flow, focus on the overall mechanical system to prevent damage and allow for successful operation is critical. Unique to sCO_2 systems is the complex packaging required to fit all components: bearings, seals, variable IGVs, pressure containment, and manifolds / ports for all internal support systems. Rotordynamics and pressure containment are mechanical challenges, and careful consideration is required to balance out both. As there is continued development in CCS technologies, continuing to pursue the development of high-flow sCO_2 compressors will reduce OPEX and CAPEX of carbon capture and will be a necessary technology. There are still areas that require focus, primarily in aerodynamic performance and measurements at near-dome conditions [28], and the testing of mechanically reliable equipment in this area will continue to improve these uncertainties.

REFERENCES

[1] Moore, J.J., Lerche, A., Delgado, H., Allison, T., Pacheco, J., 2011, Development of Advanced Centrifugal Compressors and Pumps for Carbon Capture and Sequestration Applications, *Proceedings of the Fortieth Turbomachinery Symposium*, September 12-15, 2011, Houston, Texas.

[2] Moore, J.J., Camatti, M., Smalley, A.J., Vannini, G.V., Vermin, L.L., 2006, Investigation of a Rotordynamic Instability in a High Pressure Centrifugal Compressor Due to Damper Seal Clearance Divergence, 7th International Conference on Rotor Dynamics, September 25-28, 2006, Vienna, Austria.

[3] Lambruschini, F., Liese, E., Zitney, S., and Traverso, A., 2016, "Dynamic Model of a 10 MW Supercritical CO_2 Recompression Brayton Cycle," *ASME Turbo Expo 2016: Turbomachinery Technical Conference and Exposition*, Seoul, South Korea.

[4] Bryant, J., Saari, H., and Zanganeh, K., 2011, "An Analysis and Comparison of the Simple and Recompression Supercritical CO_2 Cycles," *Supercritical CO_2 Power Cycle Symposium*, Boulder, Colorado, United States.

[5] McClung, A., Smith, N., Allison, T., and Tom, B., 2018, "Practical Considerations for the Conceptual Design of an sCO_2 Cycle," *6th International Supercritical CO_2 Power Cycles Symposium*, Pittsburgh, Pennsylvania, United States.

[6] McClung, A., Smith, N., Allison, T., and Tom, B., 2018, "Practical Considerations for the Conceptual Design of an sCO_2 Cycle," *6th International Supercritical CO_2 Power Cycles Symposium*, Pittsburgh, Pennsylvania, United States.

[7] Moore, J.J., Evans, N., Brun, K., Kalra, C., 2015, "Development of 1 MWe Supercritical CO_2 Test Loop," *Proceedings of the ASME Turbo Expo*, Paper #GT2015-43771, June 15-19, 2015, Montreal, Quebec, Canada.

[8] Hexemer, M, 2014, "Supercritical CO_2 Brayton Recompression Cycle Design and Control Features to Support Startup and Operation," *The 4th International Symposium – Supercritical CO_2 Power Cycles: Technologies for Transformational Energy Conversion*, Pittsburgh, Pennsylvania, USA.

[9] Spadacini, C., Pesatori, E., Centemeri, Lazzarin, N., Macchi, R., and Sanvito, M., 2018, "Optimized Cycle and Turbomachinery Configuration for an Intercooled, Recompressed sCO_2 Cycle," *The 6th International Supercritical CO_2 Power Cycles. Symposium*, Pittsburgh, Pennsylvania, United States

[10] Noall, J. and Pash, J., 2014, "Achievable Efficiency and Stability of Supercritical CO_2 Compression Systems," *Supercritical CO_2 Power Cycle Symposium*, Pittsburgh, Pennsylvania, United States.

[11] Monge, B., Sanchez, D., Savill, M., and Sanchez, T., 2014, "Exploring the Design Space of the sCO_2 Power Cycle Compressor," *The 4th International Symposium – Supercritical CO_2 Power Cycles*, Pittsburg, Pennsylvania, United States.

[12] Wacker, C. and Dittmer, R, 2014, "Integrally Geared Compressors for Supercritical CO_2," *The 4th International Symposium – Supercritical CO_2 Power Cycles*, Pittsburgh, Pennsylvania, United States.

[13] Schuster, S., Benra, F., and Brillert, D., 2016, "Small Scale sCO_2 Compressor Impeller Design Considering Real Fluid Conditions," *The 5th International Symposium – Supercritical CO_2 Power Cycles*, San Antonio, Texas, United States.

[14] Del Greco, A. and Tapinassi, L., 2013, "On the Combined Effect on Operating Range of Adjustable IGVs and Variable Speed in Process Multistage Centrifugal Compressors," *ASME Turbo Expo 2013: Turbine Technical Conference and Exposition*, San Antonio, Texas, USA.

[15] Ertas, B., Delgado, A., and Moore, J., 2018, "Dynamic Characterization of an Integral Squeeze Film Bearing Support Damper for a Supercritical CO_2 Expander," *Journal of Engineering for Gas Turbines and Power*.

[16] Cich, S., Moore, J., Kulhanek, C., and Mortzheim, J., "Development and Testing of a Supercritical CO2 Compressor Operating Near the Dome," *Turbomachinery & Pump Symposium*, December 2020.

[17] Cich, S., Moore, J., Mortzheim, J., and Hofer, D, 2018, "Design of a Supercritical CO_2 Compressor for use in a 10 MWe Power Cycle," *The 6th International Supercritical CO_2 Power Cycles Symposium*, Pittsburgh, Pennsylvania, United State.

[18] Tan, J., Qi, D., and Wang, R., 2010, "The Effect of Radial Inlet on the Performance of Variable Inlet Guide Vanes in Centrifugal Compressor Stage,: *ASME Turbo Expo 2010: Power for Land, Sea, and Air*, Glasgow, UK.

[19] Sezal, I., Chen, N., Aalburg, C., Gadamsetty, R., Erhard, W., Del Greco, A., Tapinassi, L., and Lang, M., 2016, "Introduction of Circumferentially Non-uniform Variable Guide Vanes in the Inlet Plenum of a Centrifugal Compressor for Minimum Losses and Flow Distortion," *Journal of Turbomachinery*, September 2016, Vol. 138.

[20] Cich, S., Moore, J., Towler, M., Mortzheim, J., and Hofer, D., 2019, "Loop Filling and Start Up with a Closed Loop sCO_2 Brayton Cycle," *ASME 2019 Turbo Expo*, Phoenix, Arizona, United States.

[21] Ameridrives Alta Industrial Motion - “Ameriflex Diaphragm Coupling – High Speed, High Performance Design.”

[22] American Petroleum Institute, 2005, “API Standard Paragraphs Rotordynamic Tutorial: Lateral Critical Speeds, Unbalance Response, Stability, Train Torsionals, and Rotor Balancing,” 684 ed. 2.

[23] Beardmore, R., 2013, “Loaded Flat Plate,” http://www.roymech.co.uk/Useful_Tables/Mechanics/Plates.html.

[24] Tan, J., Qi, D., and Wang, R., 2010, “The Effect of Radial Inlet on the Performance of Variable Inlet Guide Vanes in Centrifugal Compressor Stage,: ASME Turbo Expo 2010: Power for Land, Sea, and Air, Glasgow, UK.

[25] Sezal, I., Chen, N., Aalburg, C., Gadamsetty, R., Erhard, W., Del Greco, A., Tapinassi, L., and Lang, M., 2016, “Introduction of Circumferentially Non-uniform Variable Guide Vanes in the Inlet Plenum of a Centrifugal Compressor for Minimum Losses and Flow Distortion,” Journal of Turbomachinery, September 2016, Vol. 138.

[26] Cich, S., Moore, J., Kulhanek, C., Towler, M., and Mortzheim, J., “Mechanical Design and Testing of a 2.5 MW sCO_2 Compressor Loop,” *ASME 2021 Turbo Expo*, June 2021.

[27] Neveu, J., Cich, S., Moore, J., and Mortzheim, J., “Operation and Control of a Supercritical CO2 Compressor,” *ASME Turbo Expo 2021*, June 2021.

[28] Mortzheim, J., Hofer, D., Priebe, S., McClung, A., Moore, J., and Cich, S., “Challenges with Measuring Supercritical CO_2 Compressor Performance when Approaching the Liquid-Vapor Dome,” *ASME Turbo Expo 2021*, June 2021.

ACKNOWLEDGEMENTS

This material is based upon work supported by the Department of Energy, Office of Energy Efficiency and Renewable Energy (EERE), under Award Number DE-EE0007109. This report was prepared as an account of work sponsored by an agency of the United States Government. Neither the United States Government nor any agency thereof, nor any of their employees, makes any warranty, express or implied, or assumes any legal liability or responsibility for the accuracy, completeness, or usefulness of any information, apparatus, product, or process disclosed, or represents that its use would not infringe privately owned rights. Reference herein to any specific commercial product, process, or service by trade name, trademark, manufacturer, or otherwise does not necessarily constitute or imply its endorsement, recommendation, or favoring by the United States Government or any agency thereof. The views and opinions of authors expressed herein do not necessarily state or reflect those of the United States Government or any agency thereof